Purification of Kraft cellulose in mild conditions using choline acetate based deep eutectic solvents.

Greta Colombo Dugoni, Andrea Mezzetta, Lorenzo Guazzelli, Cinzia Chiappe, Monica Ferro*, and Andrea Mele *

SUPPLEMENTARY INFORMATION

Table of contents

DESs CHARACTERIZATION

NMR

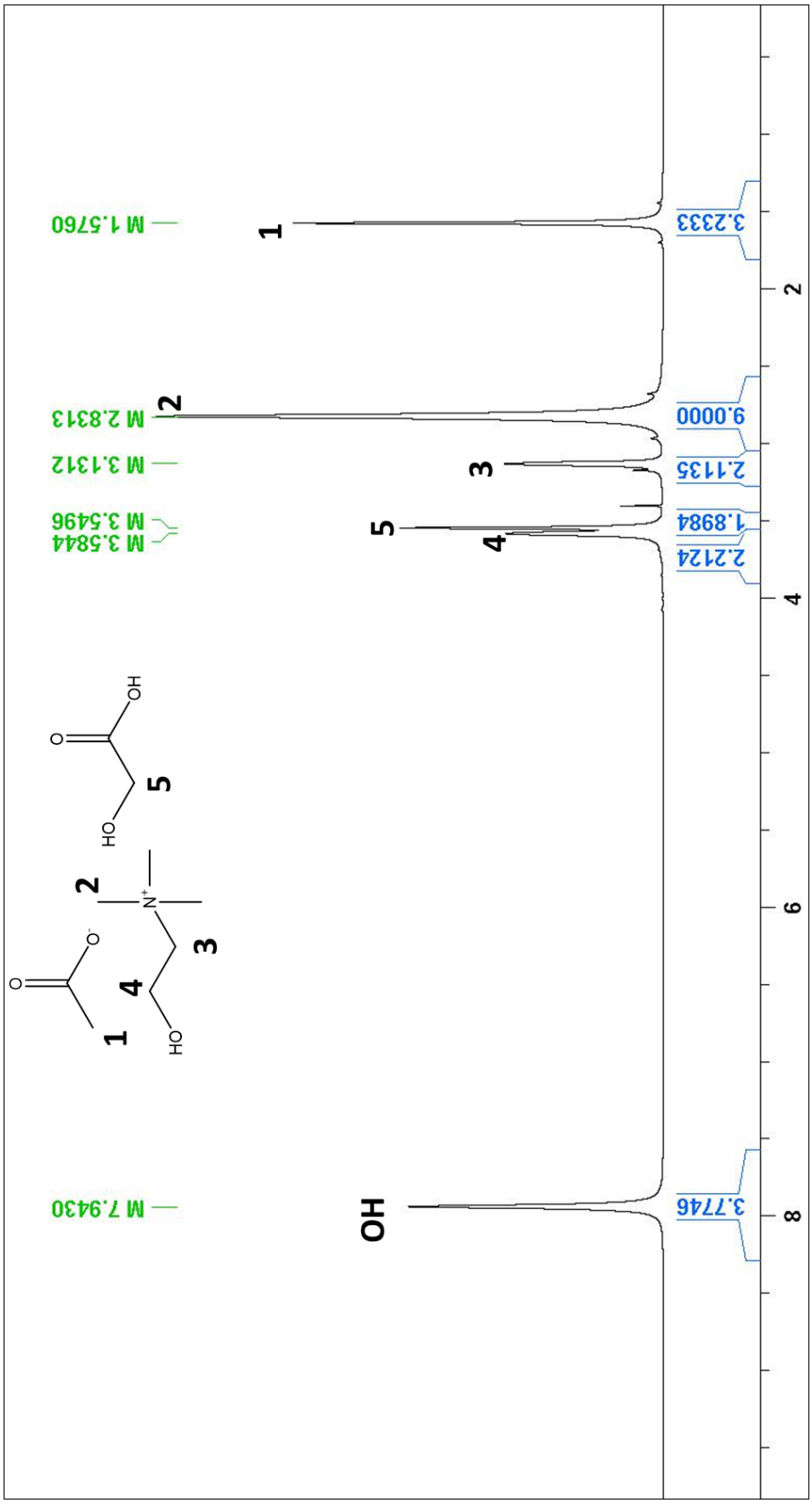

Fig. S1. ^{1}H NMR spectrum of ChOAc:GlyA

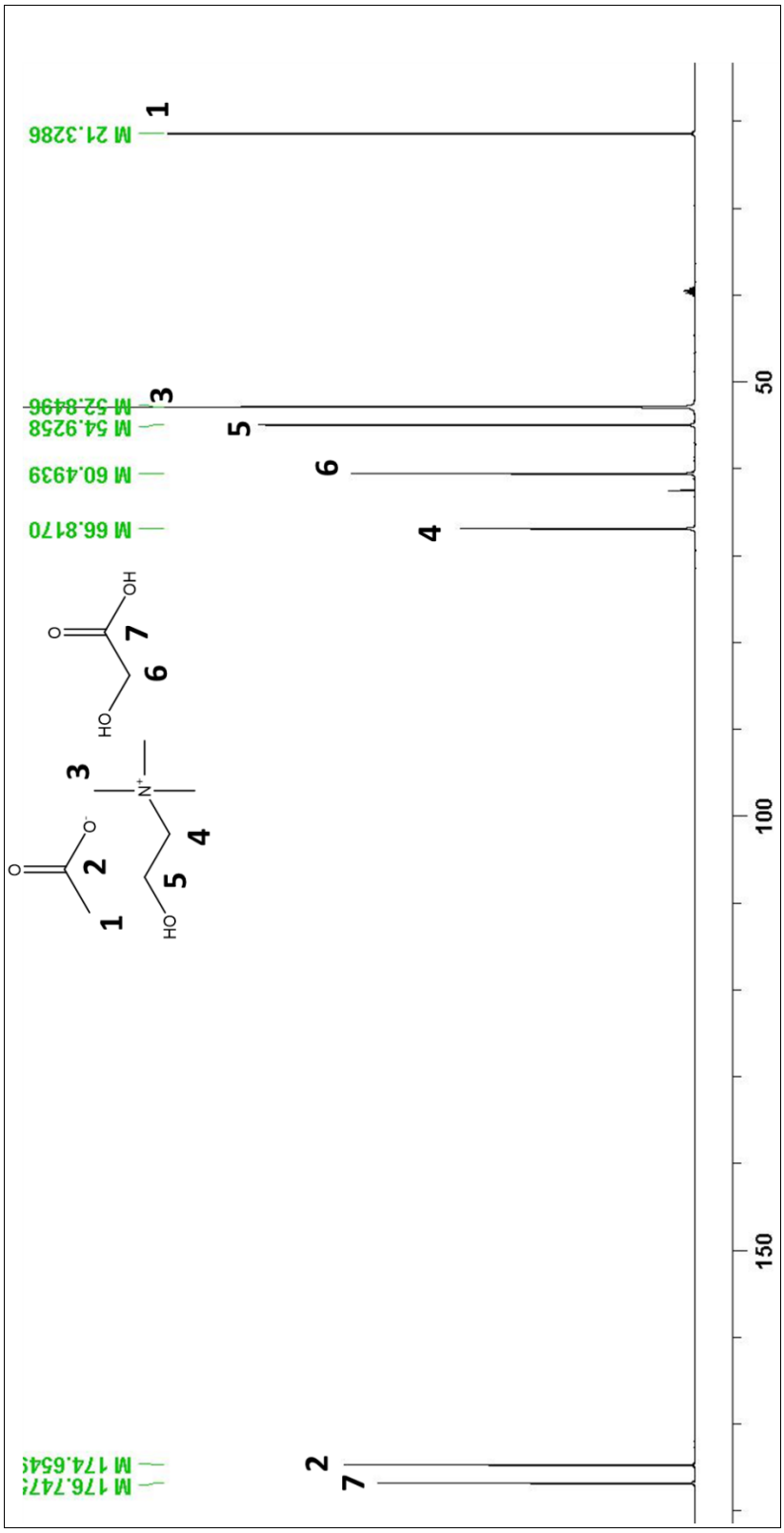

Fig. S2. ^{13}C NMR spectrum of ChOAc:GlyA

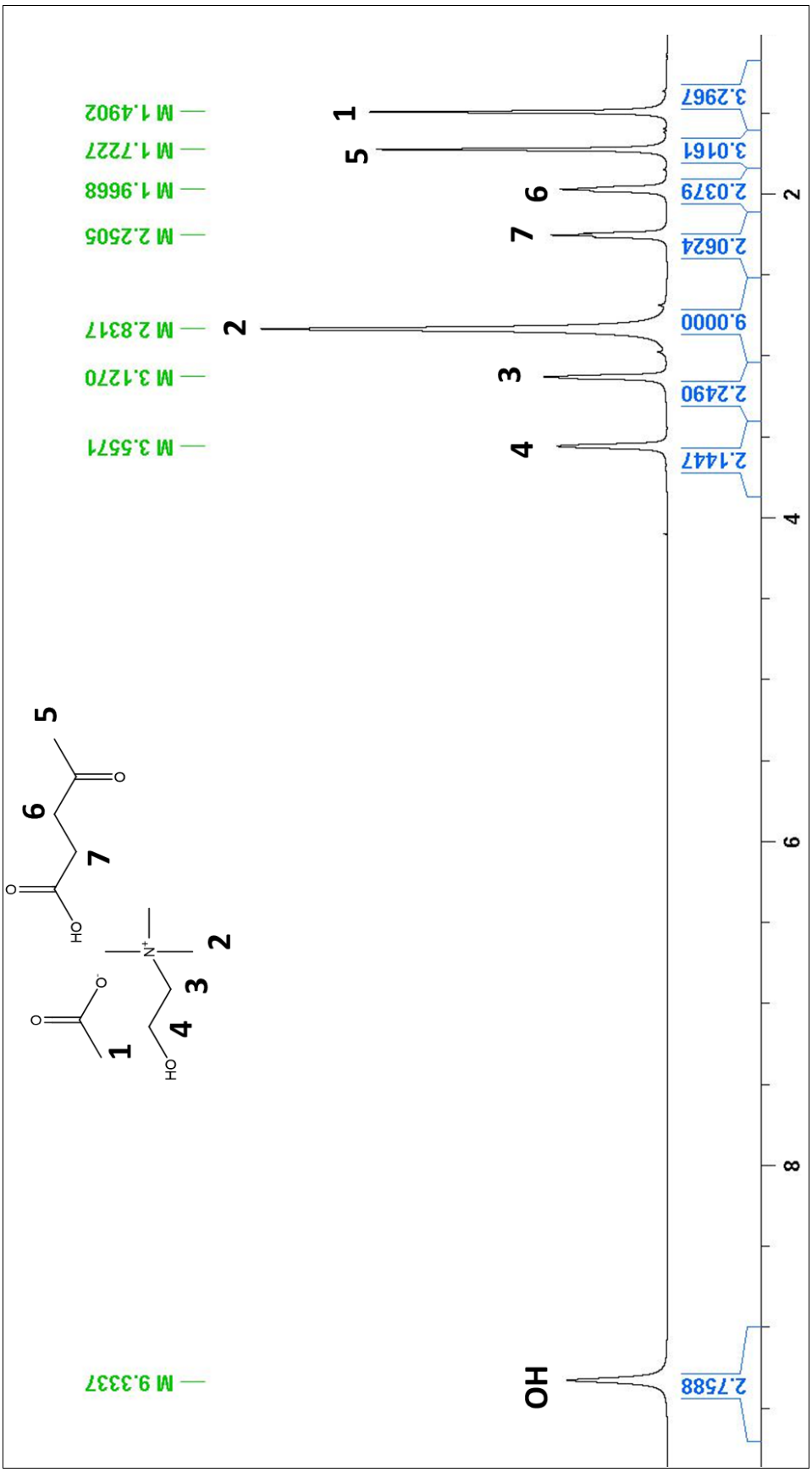

Fig. S3. ^{1}H NMR spectrum of ChOAc:LevA

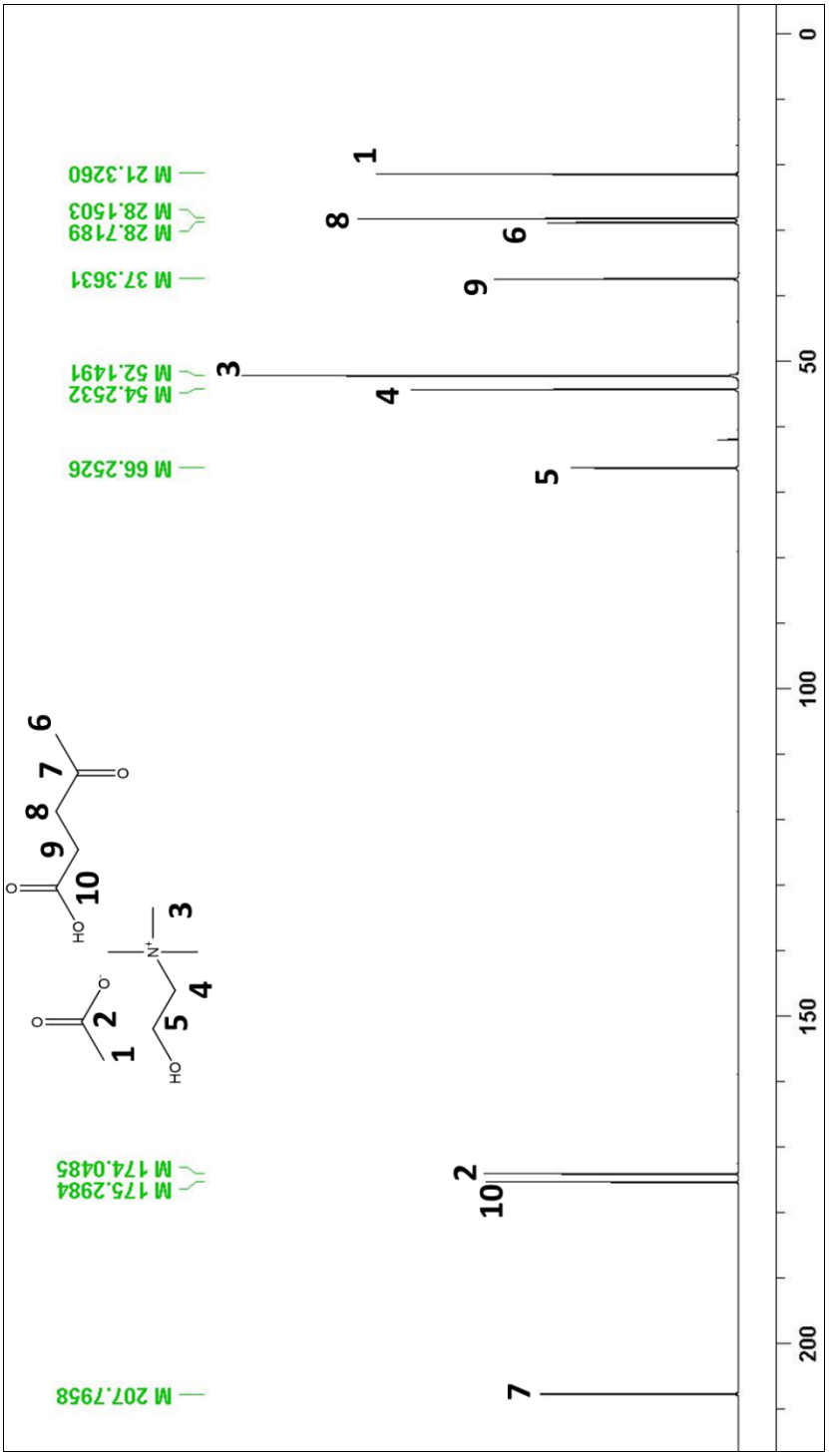

Fig. S4. ^{13}C NMR spectrum of ChOAc:LevA

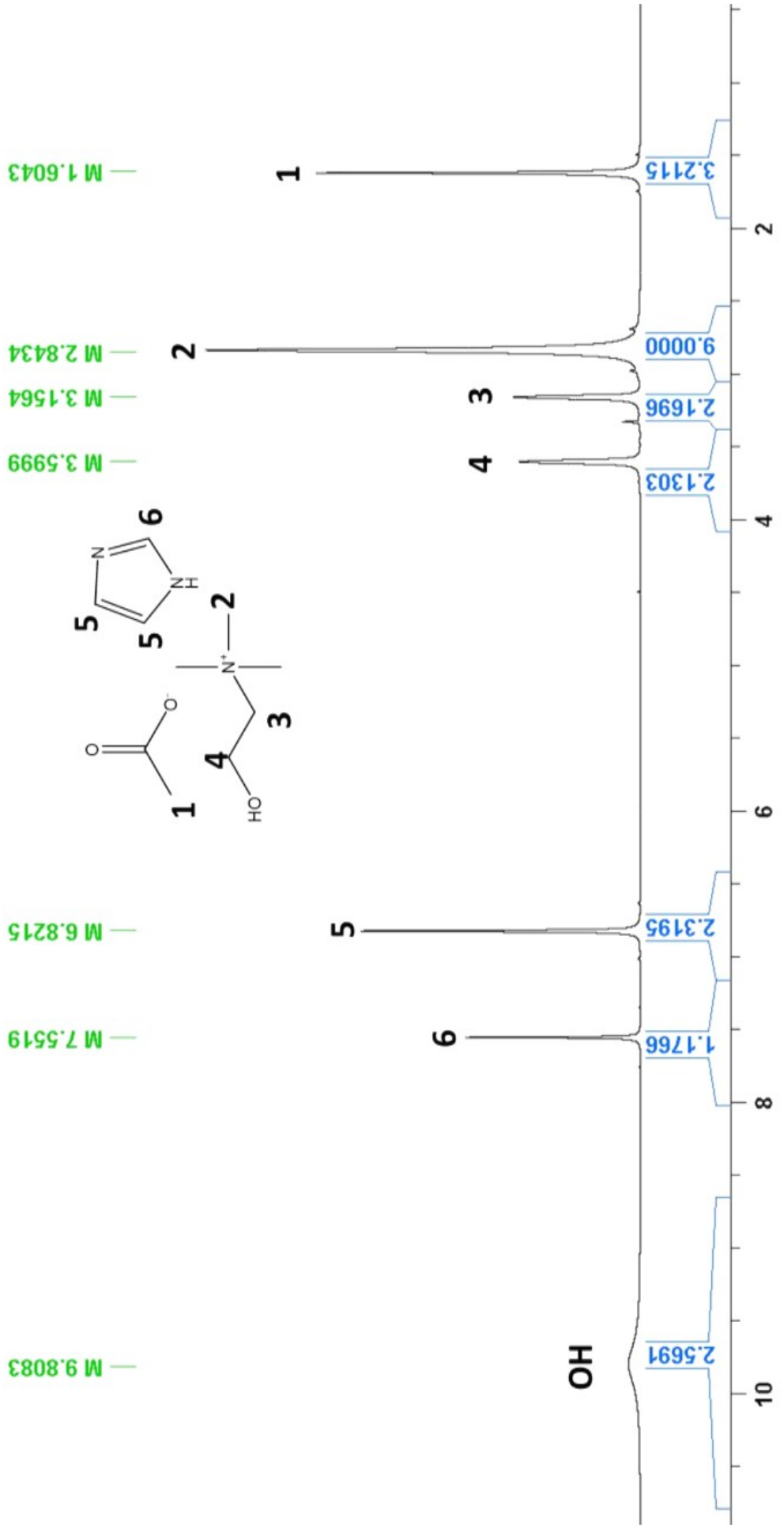

Fig. S5. ^{1}H NMR spectrum of ChOAc:Im

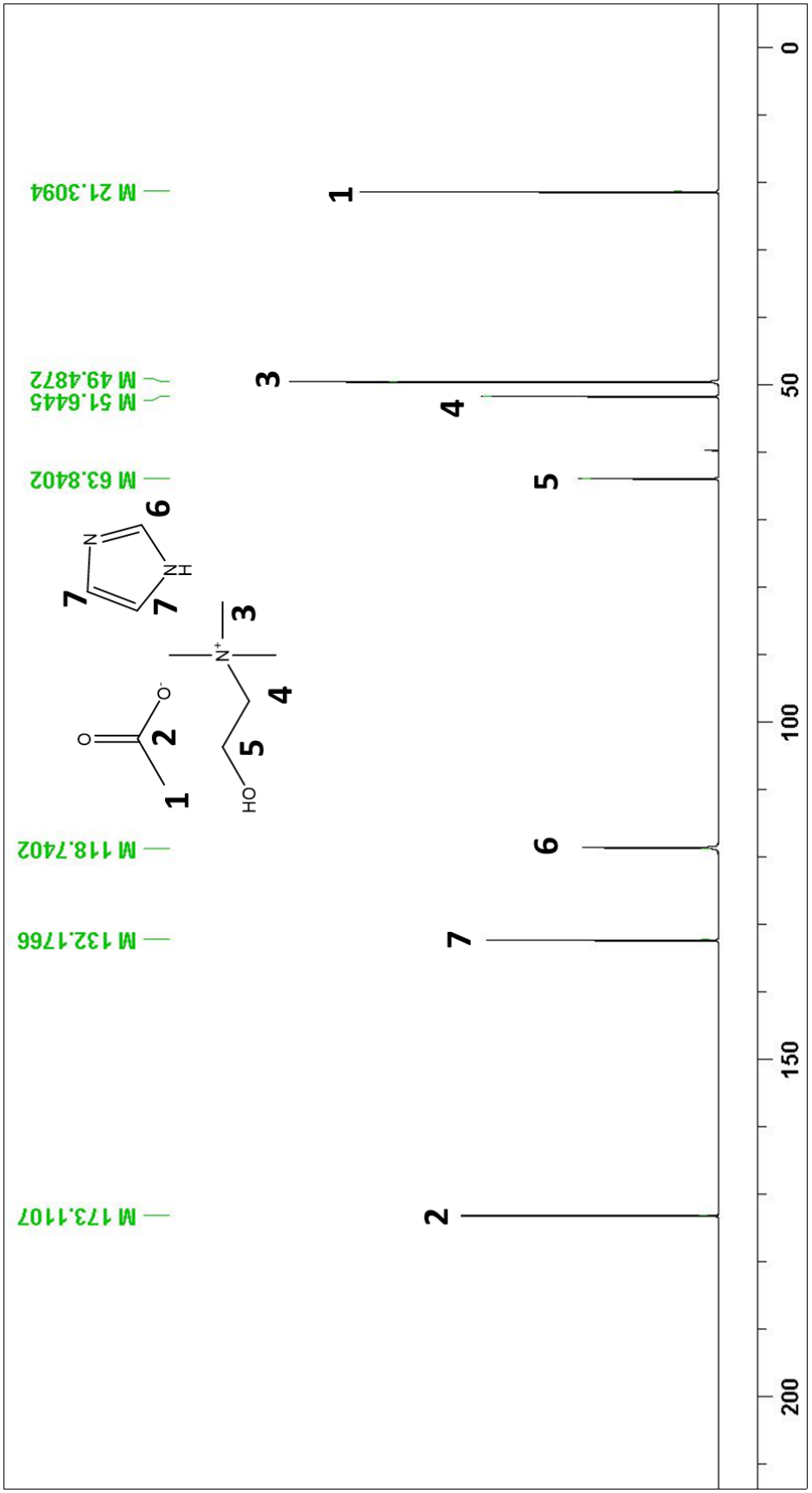

Fig. S6. ^{13}C NMR spectrum of ChOAc:Im

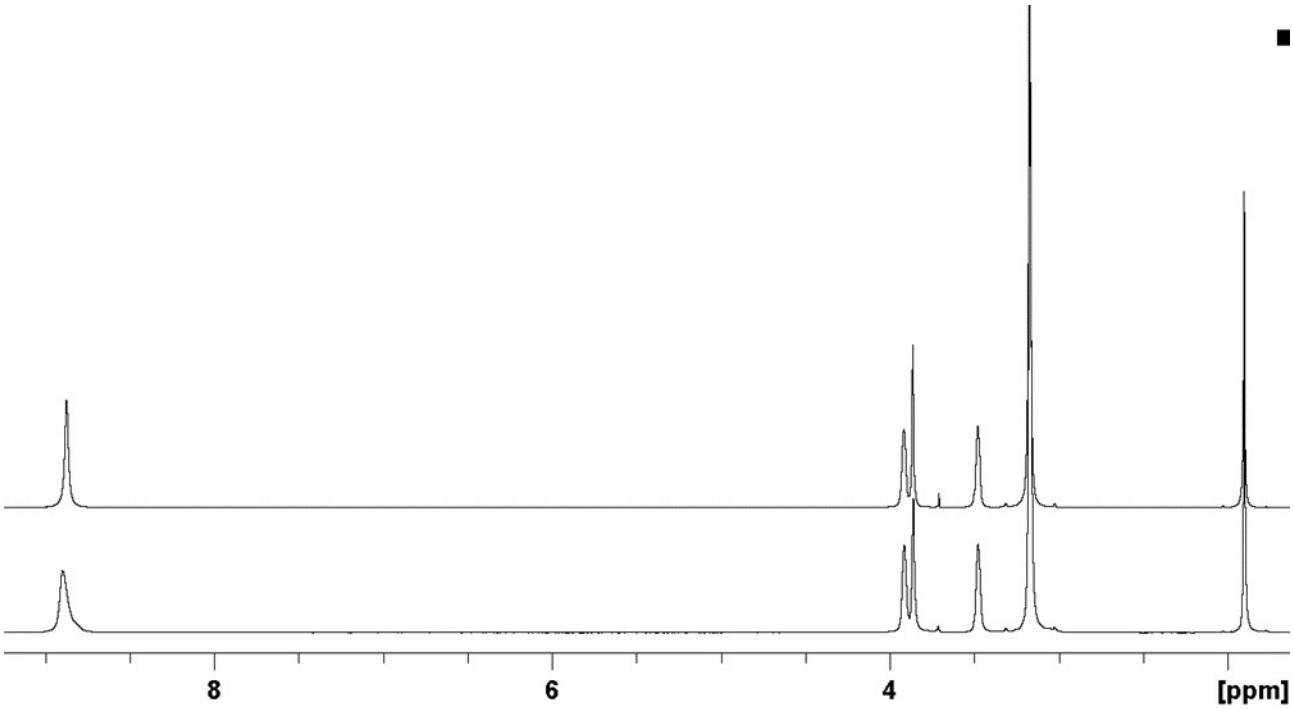

Fig. S7. ^{1}H NMR spectra of DES ChOAc:GlyA (bottom trace), and DES ChOAc:GlyA after four weeks at 25°C (top trace).

Viscosity

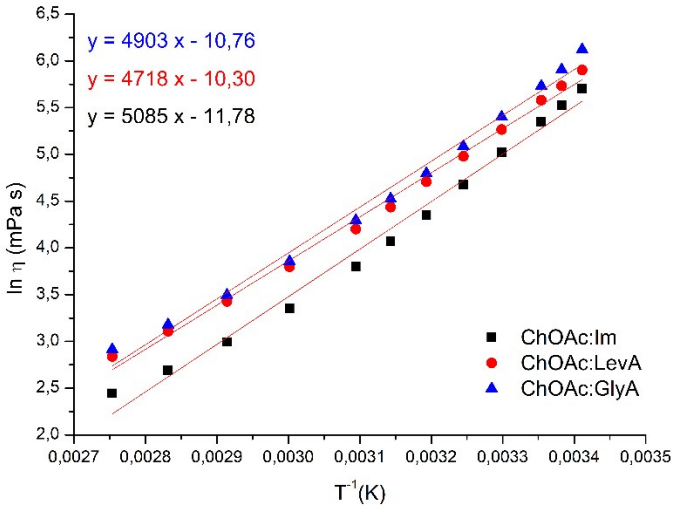

Fig. S8. Arrhenius plot of the viscosity behavior of ChOAc:LevA (red), ChOAc:Im (red), and ChOAc:GlyA (blue) as a function of temperature.

Table S1. Dependence of viscosity (mPa s) on temperature of ChOAc: LevA, ChOAc:Im, and ChOAc:GlyA.

DESs viscosity (mPa s)						
***T* (°C)**	**ChOAc:Im**		**ChOAc:LevA**		**ChOAc:GlyA**	
20	300,54	± 0,67	366,01	± 1,49	456,07	± 5,23
22,5	250,44	± 0,78	308,68	± 1,13	367,13	± 2,55
25	210,50	± 0,45	265,04	± 1,11	307,73	± 1,91
30	151,44	± 0,47	193,36	± 0,34	221,86	± 1,36
35	107,59	± 0,50	145,45	± 0,33	161,52	± 0,93
40	77,43	± 0,39	110,66	± 0,26	121,10	± 0,79
45	58,68	± 0,57	84,42	± 0,05	92,30	± 0,60
50	44,75	± 0,44	66,78	± 0,19	73,32	± 0,53
60	28,65	± 0,21	44,57	± 0,16	47,21	± 0,45
70	19,95	± 0,02	30,75	± 0,10	32,96	± 0,30
80	14,74	± 0,07	22,38	± 0,04	24,04	± 0,14
90	11,52	± 0,03	17,09	± 0,06	18,45	± 0,12

Table S2. Arrhenius model parameters for different DESs.

$$\ln \eta = \ln \eta_{\infty} + E_a/RT$$

DESs	ln η_{∞}	E_a/R	R^2	E_a (KJ/mol)	η_{∞} (mPa s)
ChOAc:GlyA	-10,76	4903	0,991	40,77	2,12 E-05
ChOAc:LevA	-10,30	4718	0,994	39,23	3,36 E-05
ChOAc:Im	-11,78	5085	0,989	42,28	7,66 E-06

DSC

The thermal behaviour of the DESs was evaluated with a differential scanning calorimeter (DSC). All DESs have been analyzed by running two cycles at different scanning rates. The obtained data are reported in Table S2. Glycolic acid and levulinic acid-based DESs present a strong tendency to form glass phases at all scanning rates used. The glass transition has been observed before for several DESs and is also present in the case of the imidazole containing DES. However, this latter also displays a melting transition in the heating run with an associated crystallization event in the cooling run. At the scanning rate of 5 °C/min, in the first cooling run, it was possible to observe a small enthalpy variation in the crystallization phenomenon and for this reason in the heating run a strong cold crystallization event was present (DSC curves are reported in the supplementary information file). Conversely, in the second cycle, the enthalpy of crystallization was higher with a consequent decrease of the cold crystallization event. At 2 °C/min the imidazole-based DES shows a typical low melting salt behavior with only one crystallization event in the cooling run and a melting event in the heating run.

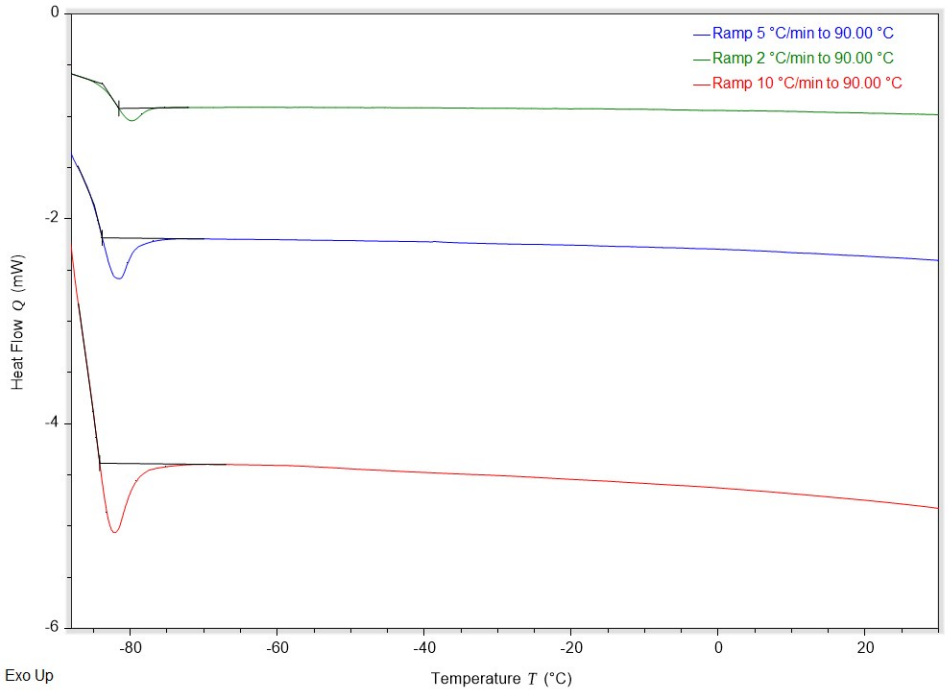

Fig. S9. DSC of DES ChOAc:GlyA 1:1

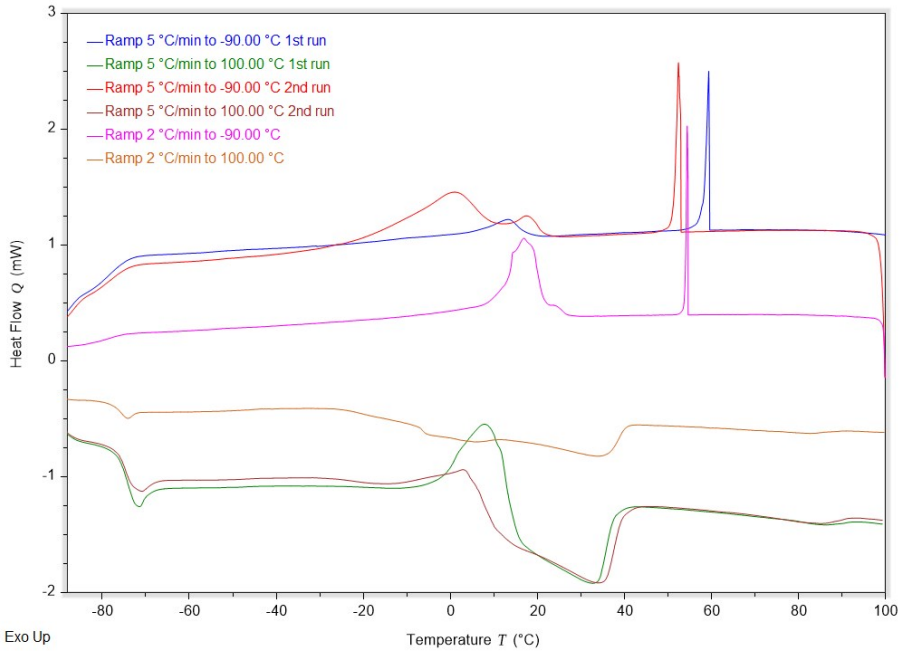

Fig. S10. DSC of DES ChOAc:Im 1:1

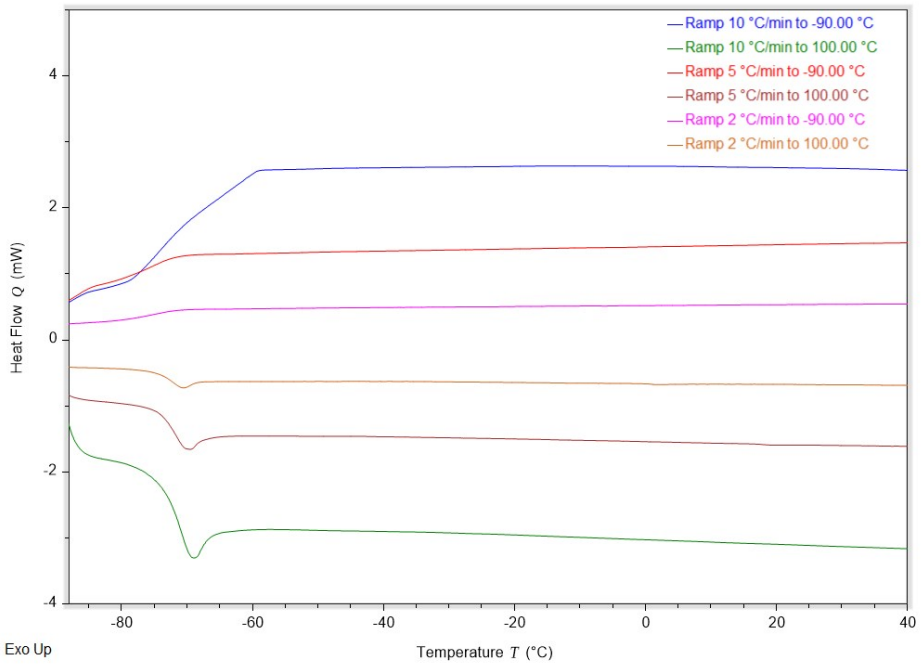

Fig. S11. DSC of DES ChOAc:LevA 1:1

Table S3. Crystallization (Tc), glass transition (Tg), cold crystallization (Tcc), and melting (Tm) temperatures for the prepared DES.

	1° Cycle				
	Cooling		Heating		
DES	**T_c**	**T_g**	**T_g**	**T_{cc}**	**T_m**
ChOAc:GlyA			-84.60[a]		
			-84.39[b]		
			-82.70[c]		
ChOAc:Im	17.83[b,d]	-78.95[c]	-75.11[b,d]	-2.78[b,d]	13.50[b,d]
	22.05[b]		-75.07[b]	-9.75[b]	7.57
	21.51[c]		-77.11[c]		-12.18[c]
ChOAc:LevA		-75.06[b]	-75.57[a]		
		-75.50[c]	-72.89[b]		
			-73.47[c]		

[a] scanning rate 10 °C/min. [b] scanning rate 5 °C/min. [c] scanning rate 2 °C/min. [d] 2nd cycle

TGA

The thermal stability of the DESs was investigated by thermal gravimetric analysis (TGA), conducted in a TA Instruments Q500 TGA. The short-term stability of choline OAc based-DESs was evaluated in ramp mode at 10 °C/min under nitrogen atmosphere (90 mL/min). As reported in recent papers [1,2], the thermal stability of a DES depends on both the nature of the constituting HBA and HBD, and the strength of the hydrogen bonds between them. When the temperature reaches a specific point, the hydrogen bonds can be broken and the compound with relatively poor thermal stability will decompose at (or close to) its characteristic decomposition temperature followed by the remaining component. For ChOAc:GlyA DES, two decomposition steps can be noted, with the evaporation/decomposition of HBD occurring at lower temperature, followed by the degradation of ChOAc. Imidazole and levulinic acid-based DESs present instead a single degradation event attributable to both HBD and HBA degradations. On the basis of onset temperatures, the thermal stability of the levulinic acid-based DES was 20 °C higher than that of the DES containing imidazole.

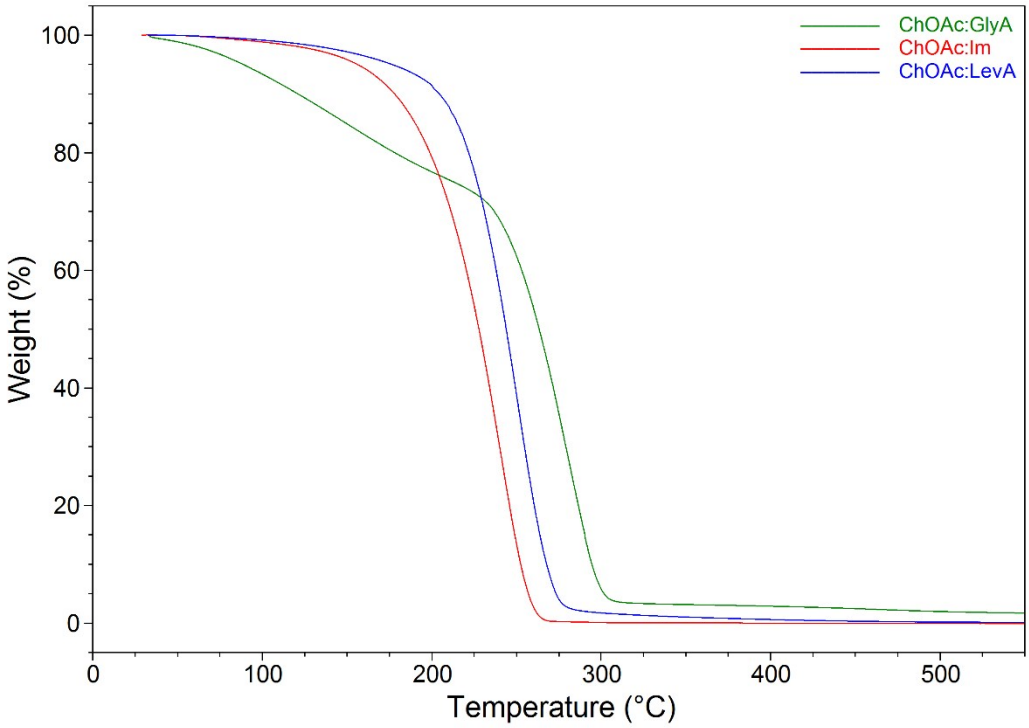

Fig. S12. Thermogravimetric curves of DESs.

Table S4. Start 5% (T_{start} 5%), onset (T_{onset}), and peak (T_{peak}) degradation temperatures for DESs.

DESs	$T_{start\ 5\%}$ (°C)	T_{onset} (°C)	T_{peak} (°C)
ChOAc:GlyA	88.75	249.8	279.1
ChOAc:LevA	176.2	220.0	250.9
ChOAc:Im	155.9	201.3	240.5

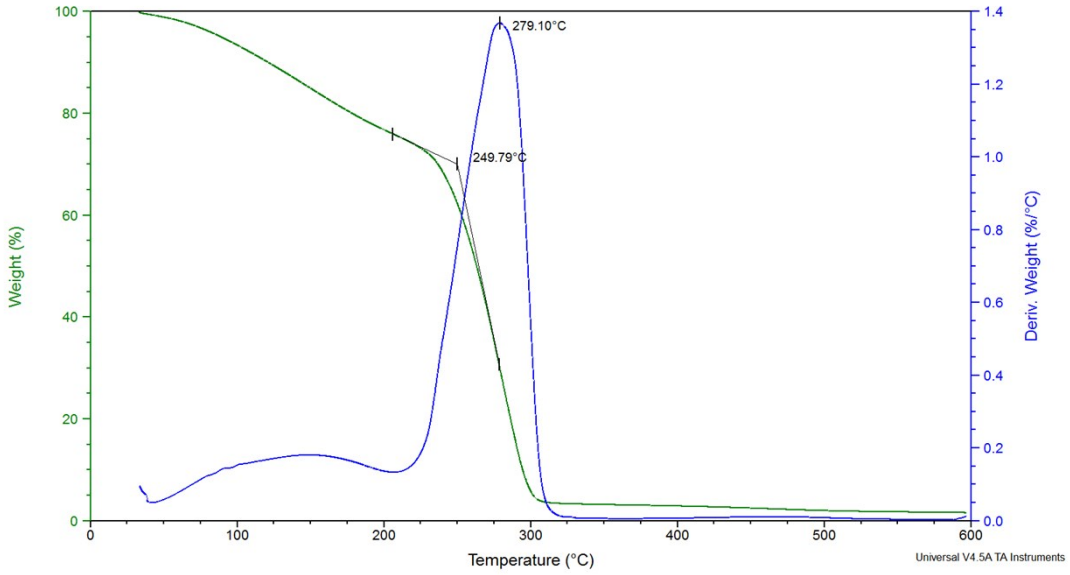

Fig. S13. TG curve of DES ChOAc:GlyA 1:1.

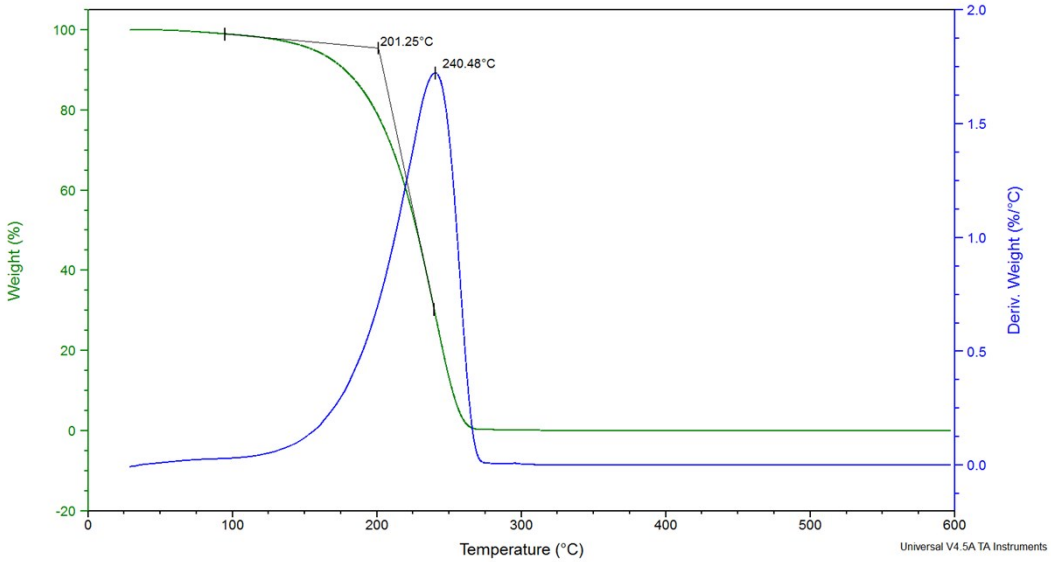

Fig. S14. TG curve of DES ChOAc:Im 1:1

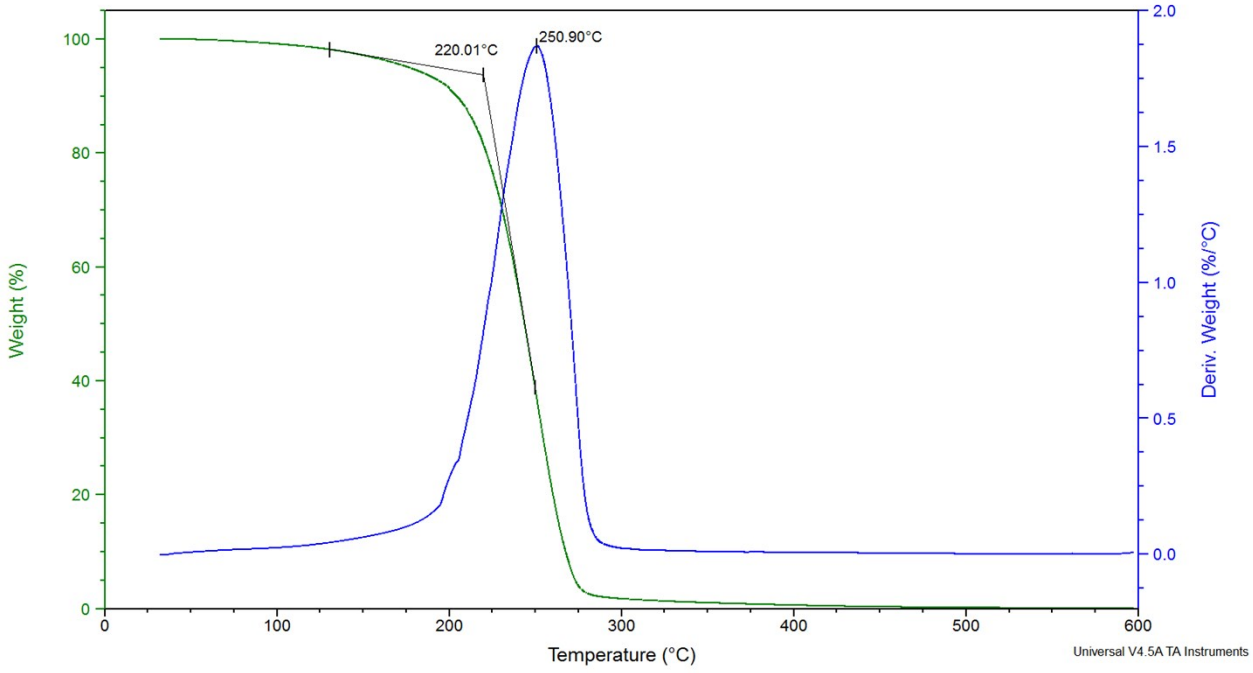

Fig. S15. TG curve of DES ChOAc:LevA 1:1

Hemicellulose solubilisation: a model study

TGA

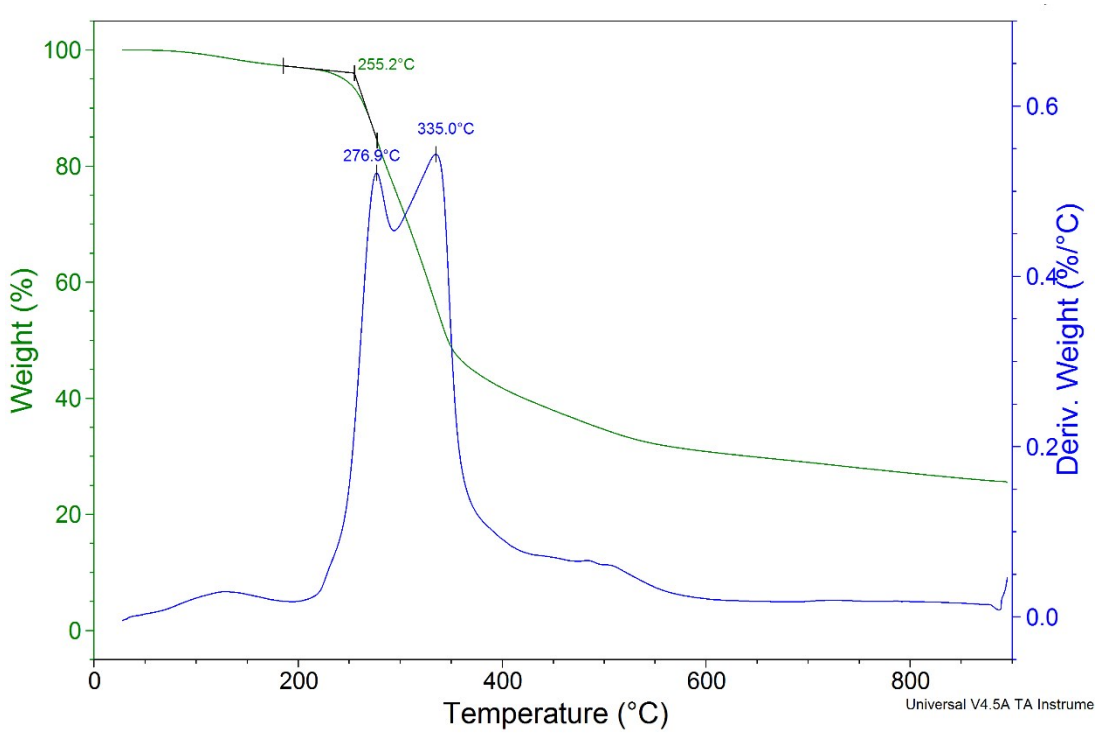

Fig. S16. TG curve of commercial hemicellulose.

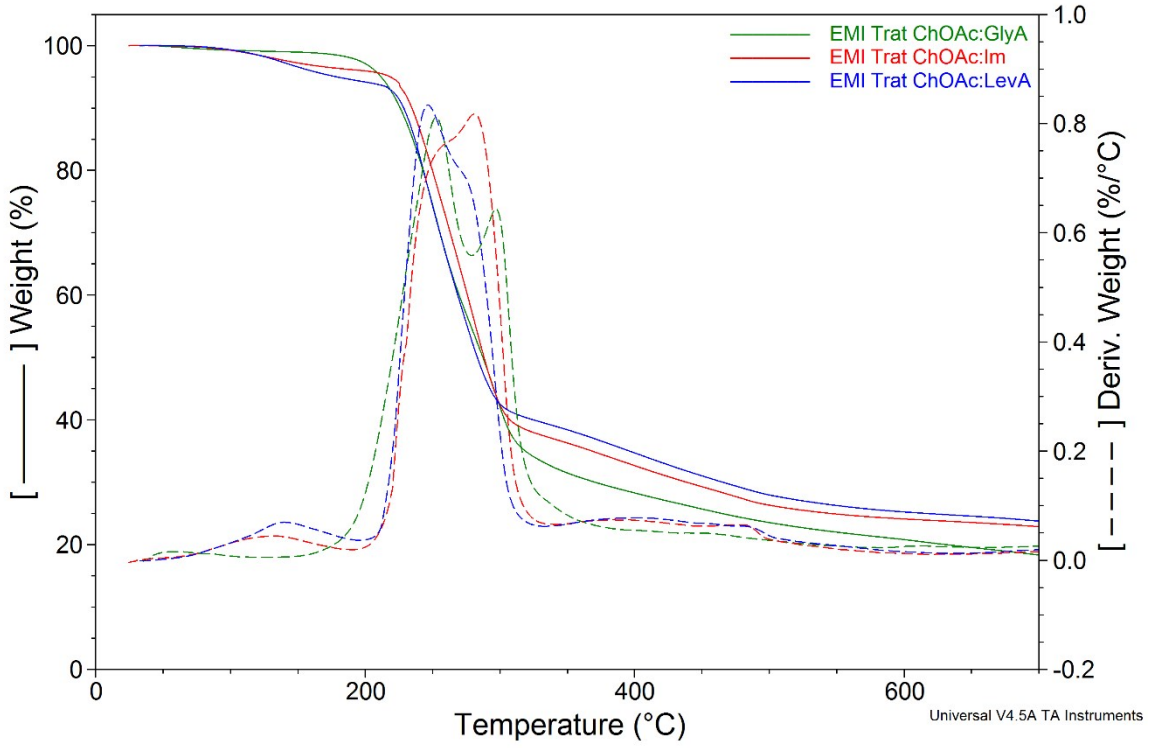

Fig. S17. TG curve of dissolved hemicellulose.

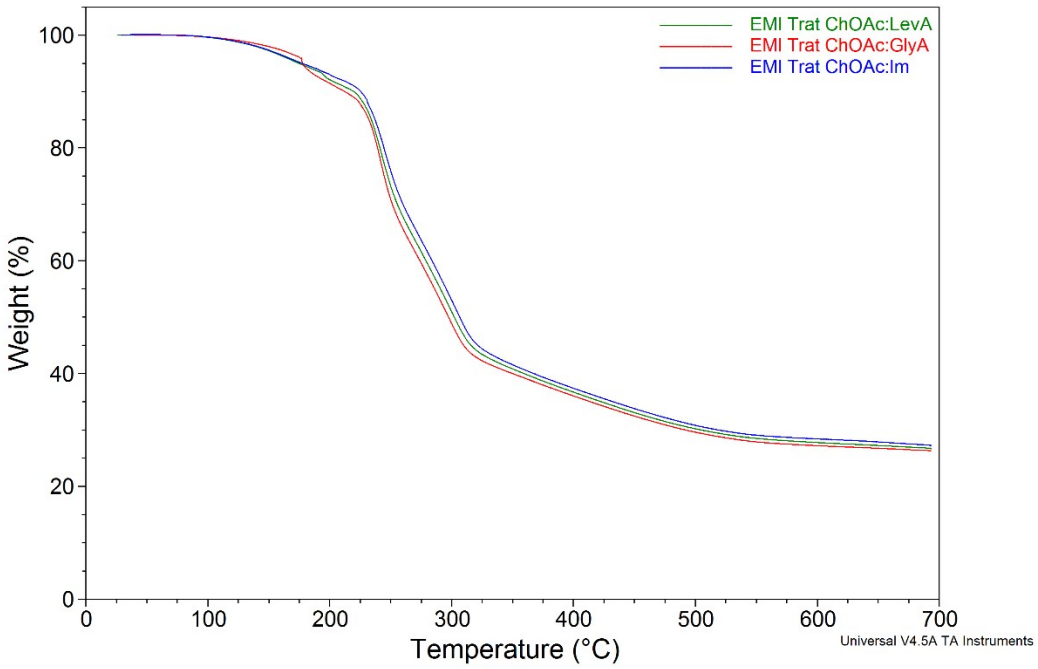

Fig. S18. TG curve of washed dissolved hemicellulose

NMR

The structure of reference hemicellulose was assessed via 2D NMR experiments such as Total Correlation Spectroscopy correlations (TOCSY) (Figure S21) and ^{13}C-^{1}H correlation (HSQC) (Figure S20). The peaks assignment based on our 2D spectra was supported by literature data, especially those published by Vignon et al.[3] Kim and Ralph[4] and Teleman et al.[5] The NMR experiments confirmed that these xylans are 4-O-Methylglucuronoxylans (GXs). This finding agrees with the most abundant type of hemicellulose known to be present in hardwood species, in our case beech. The backbone of this xylan consists of β-(1,4)-linked D-xylose units randomly substituted with 4-O-methyl-α-D-glucuronic acid residues. The structure of GXs is sketched in Figure S19.

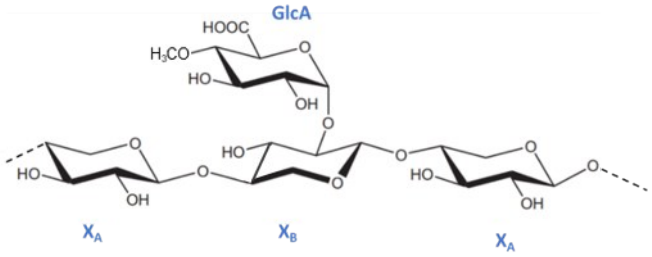

Fig. S19. Sketch of the structure of GXs and abbreviation of units.

The contour plot of HSQC is reported in Figure S20 with peak assignments.

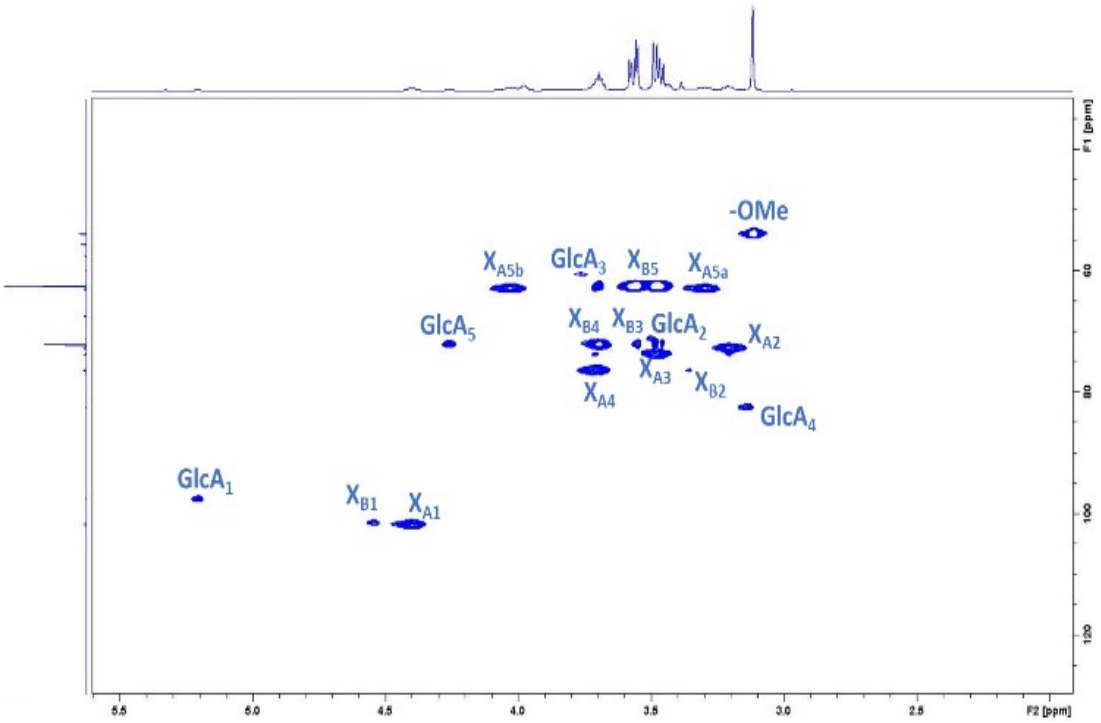

Fig. S20. Contour plot of HSQC done on GXs.

The amount of GlcA was determined by integration of the anomeric peaks and resulted about 13%.

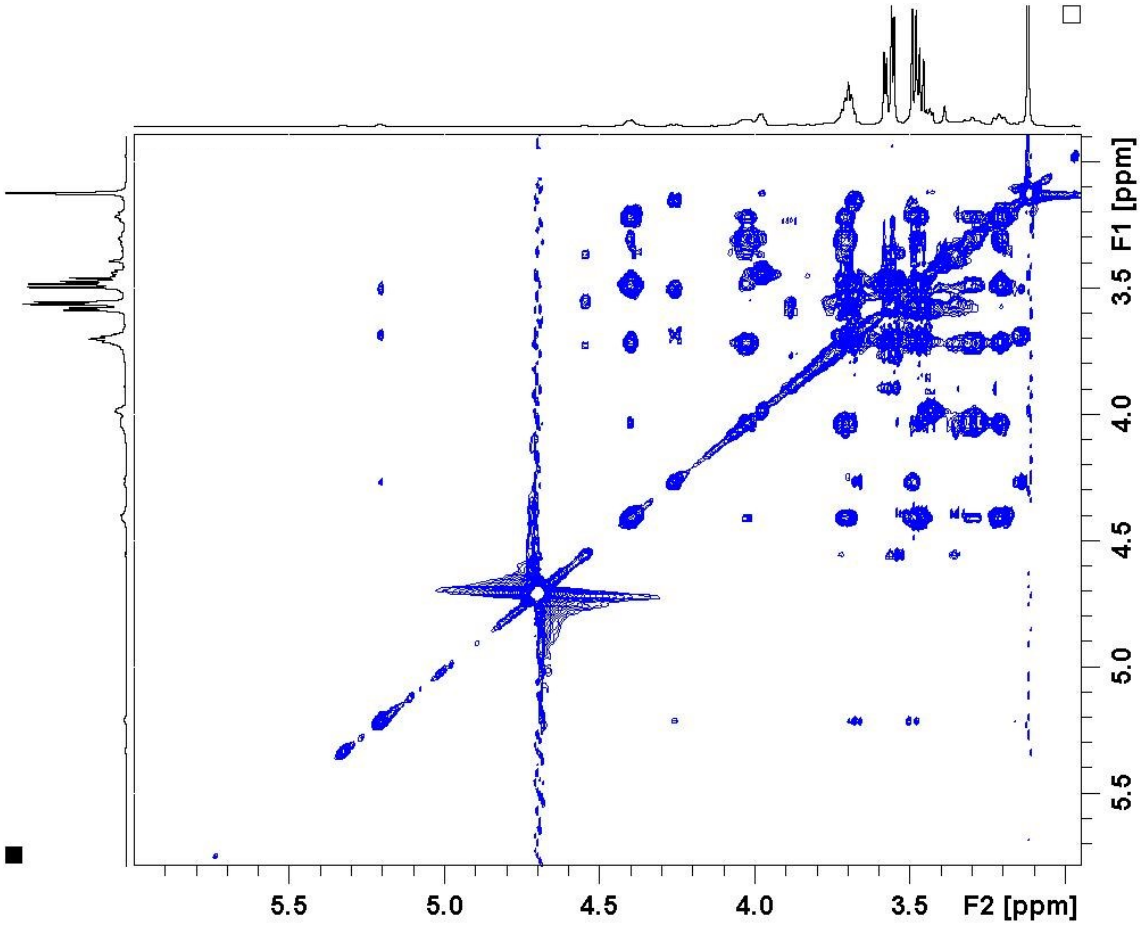

Fig. S21. TOCSY of commercial hemicellulose.

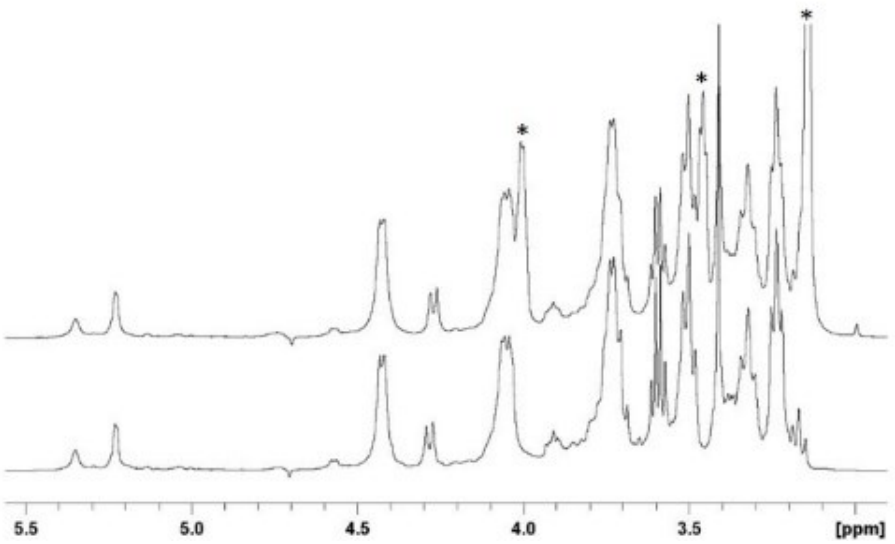

Fig. S22. Bottom trace: ^{1}H NMR spectrum of commercial hemicellulose. Top trace: ^{1}H NMR spectrum of recovered hemicellulose from DES solution after ethanol precipitation, isolation and D_2O dissolution. The asterisks show residual DES peaks.

Proof of concept: Kraft cellulose pretreatment

NMR

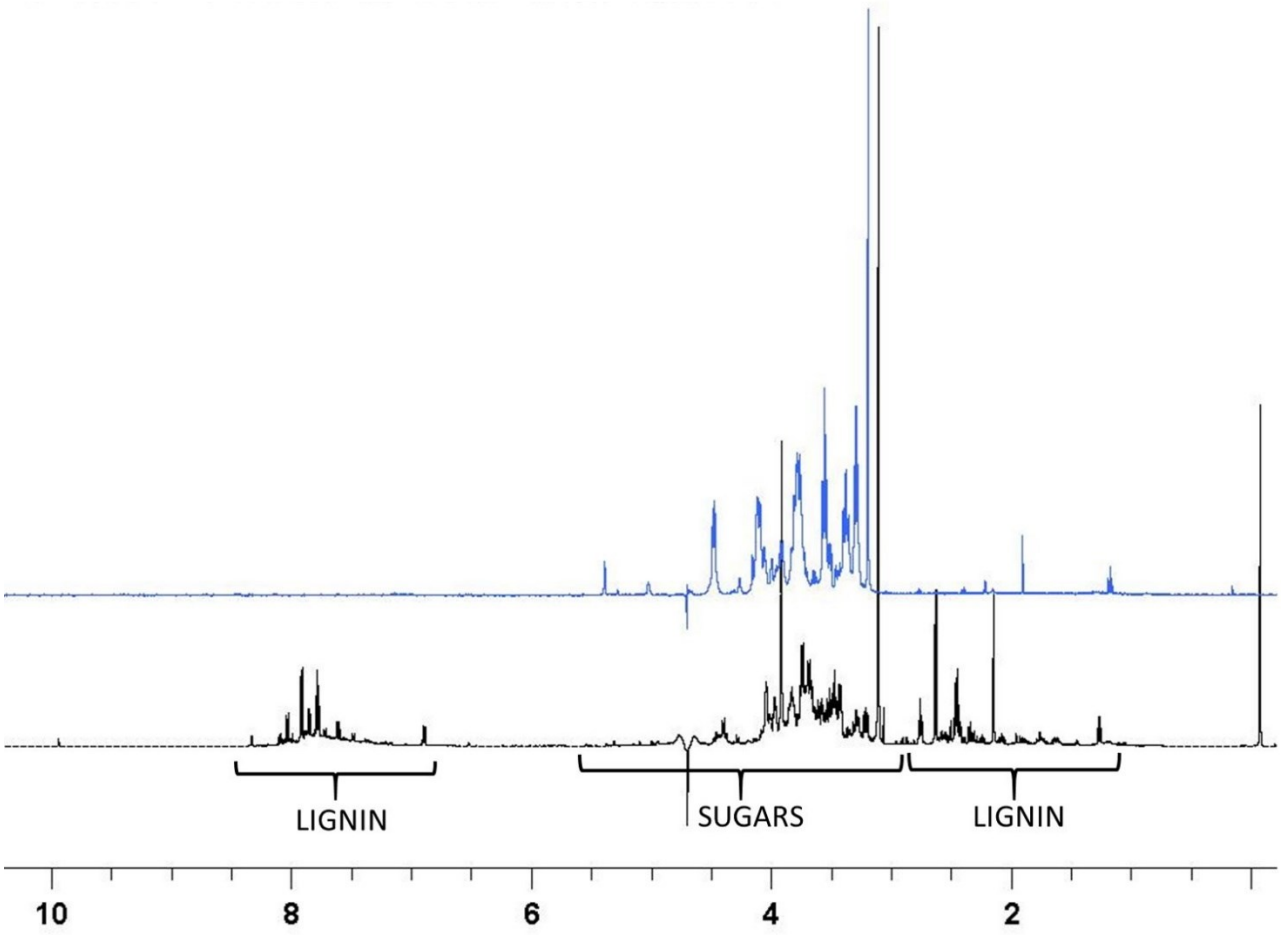

Fig. S23. Bottom trace: ^{1}H NMR spectrum of fraction extracted by alkaine treatment. Top trace: ^{1}H NMR spectrum of hemicellulose fraction from DES treatment after ethanol precipitation, drying and D_2O dissolution.

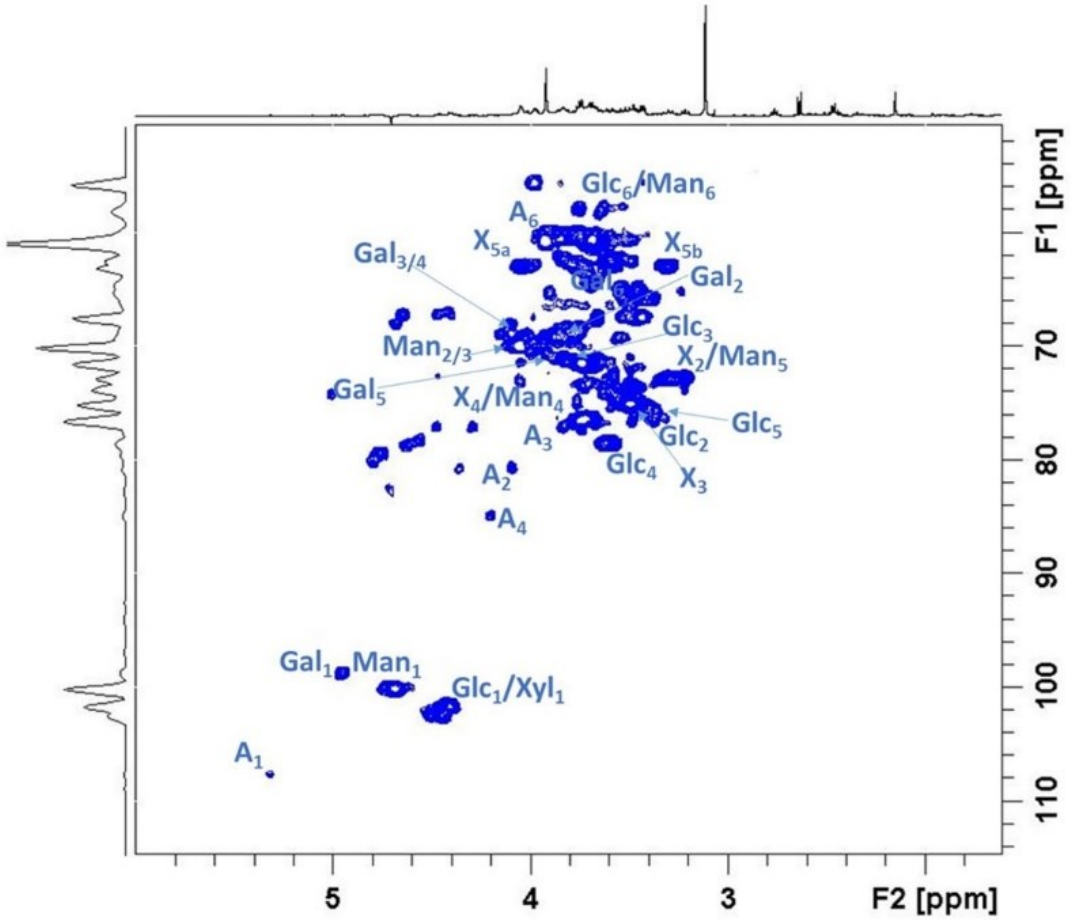

Fig. S24. HSQC of hemicellulose fraction extracted by alkaine treatment.

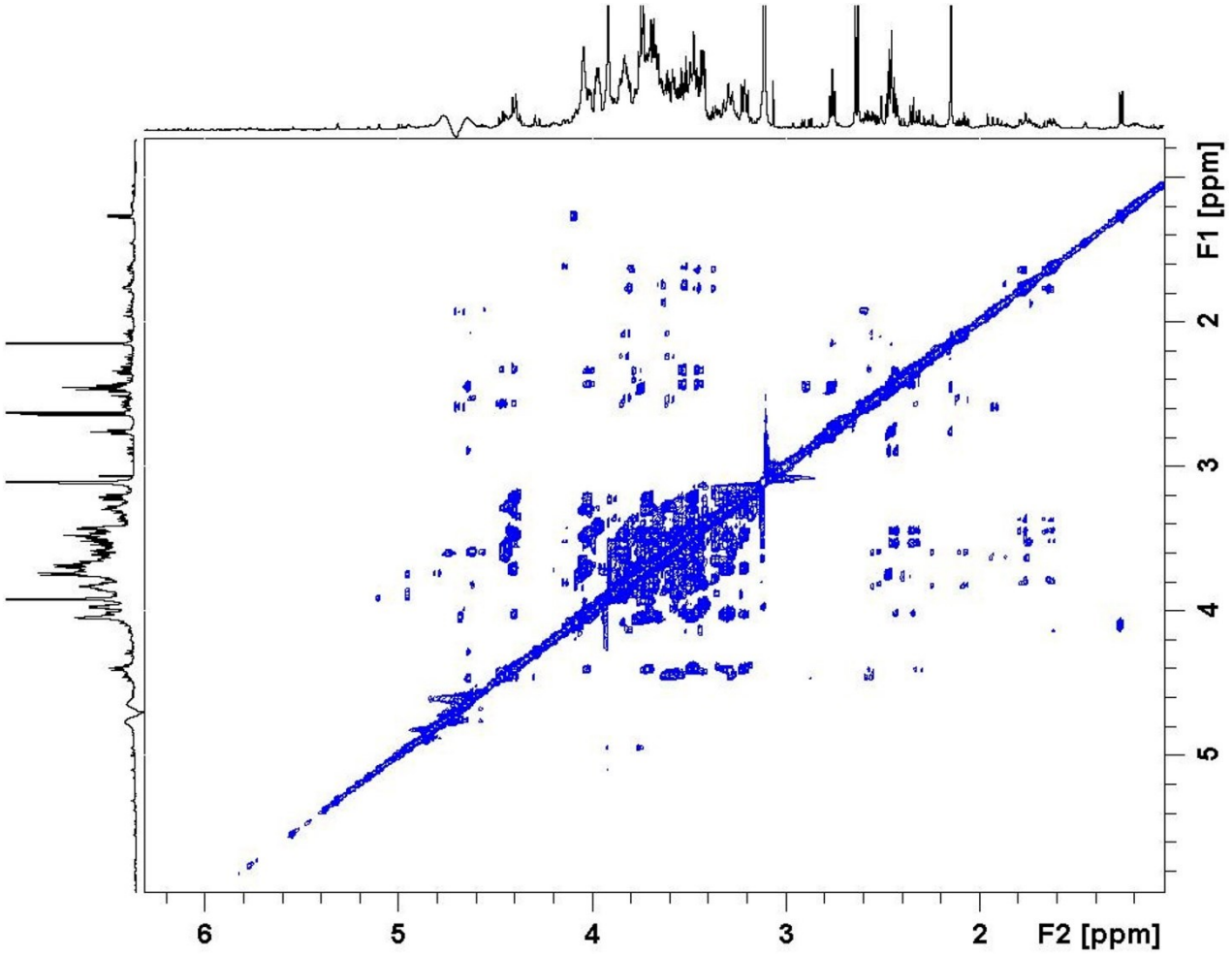

Fig. S25. TOCSY of hemicellulose fraction extracted by alkaine treatment.

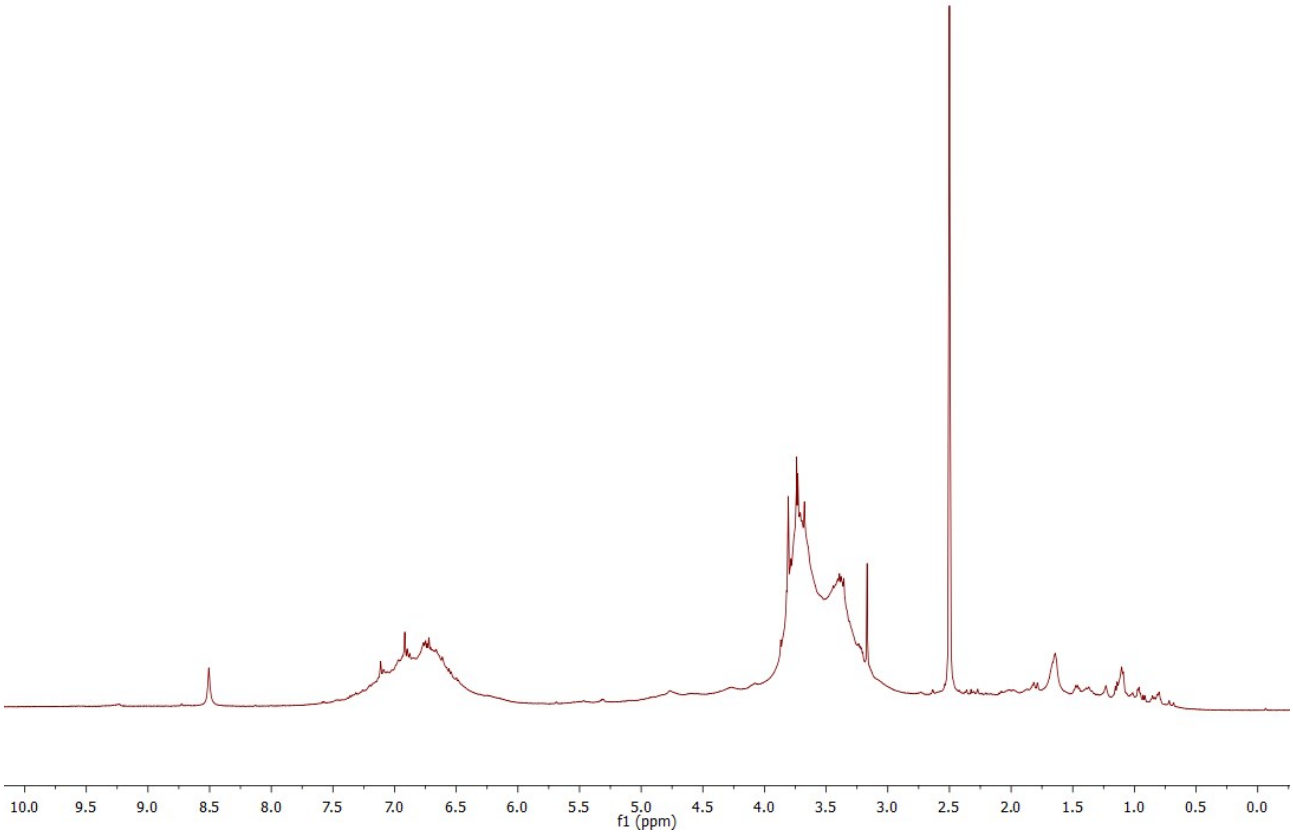

Fig. S26. ^{1}H NMR spectrum of fraction of lignin, dissolved in d6-DMSO, extracted by DES treatment.

XRD

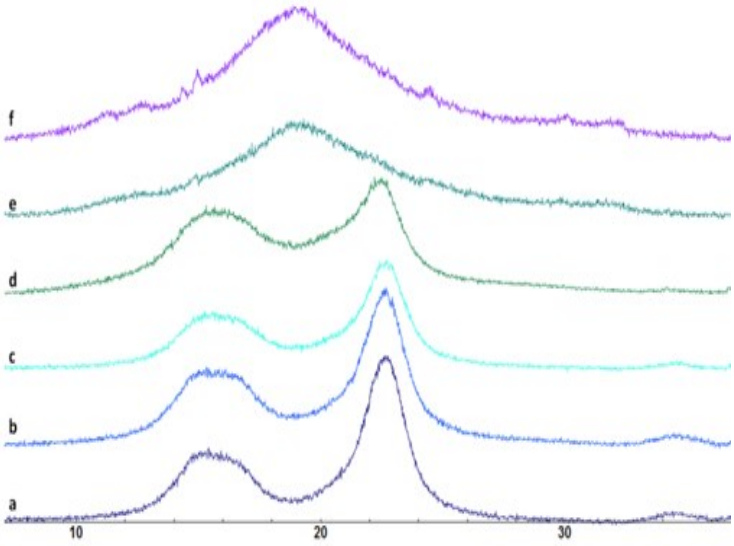

Fig. S27. Powder XRD patterns of cellulose samples before and after pretreatment with DESs. **a)** Kraft cellulose treated with ChOAc:LevA. **b)** Kraft cellulose treated with ChOAc:Im. **c)** Kraft cellulose treated with ChOAc:GlyA. **d)** Kraft cellulose. **e)** Hemicellulose extracted from Kraft cellulose. **f)** commercial hemicellulose.

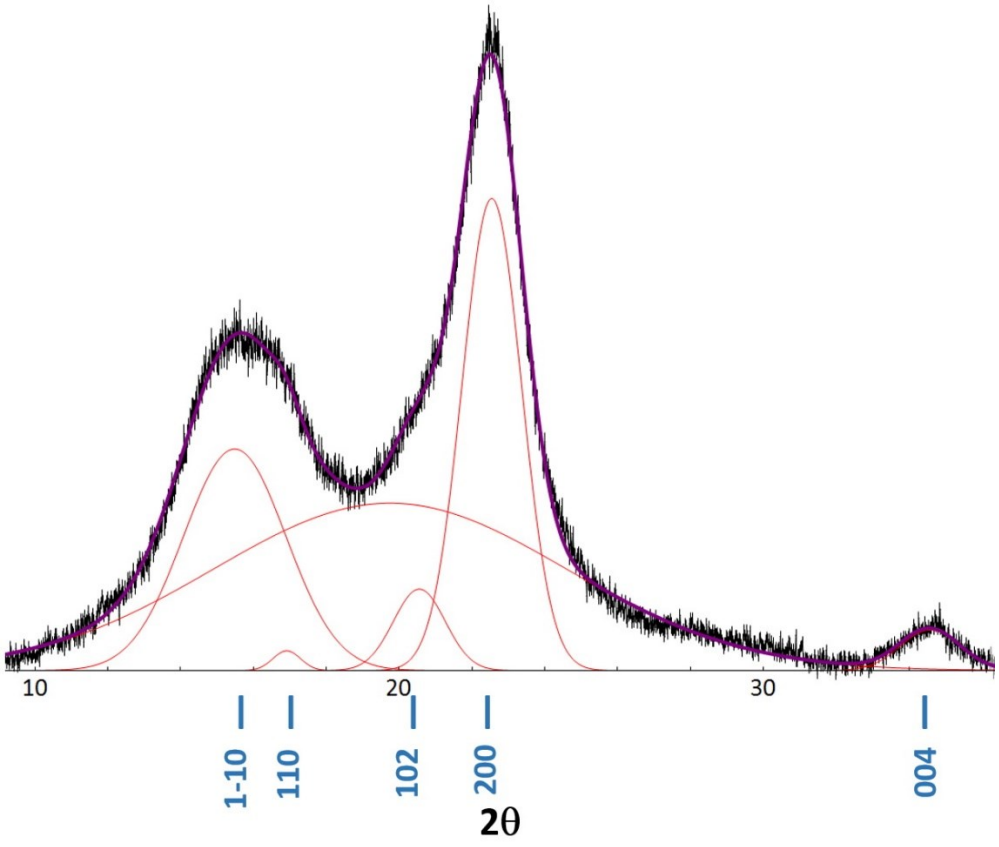

Fig. S28. XRD peaks deconvolution of pristine Kraft cellulose.

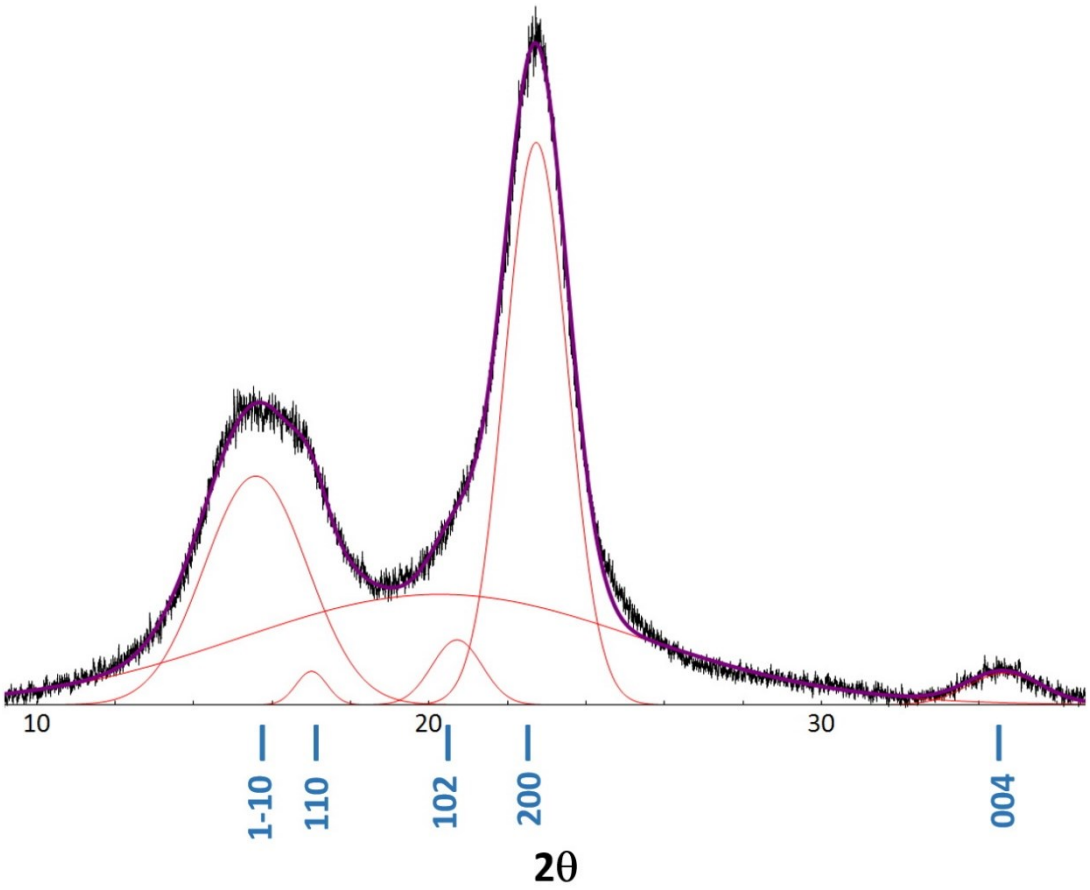

Fig. S29. XRD peaks deconvolution of Kraft cellulose treated with ChOAc:GlyA.

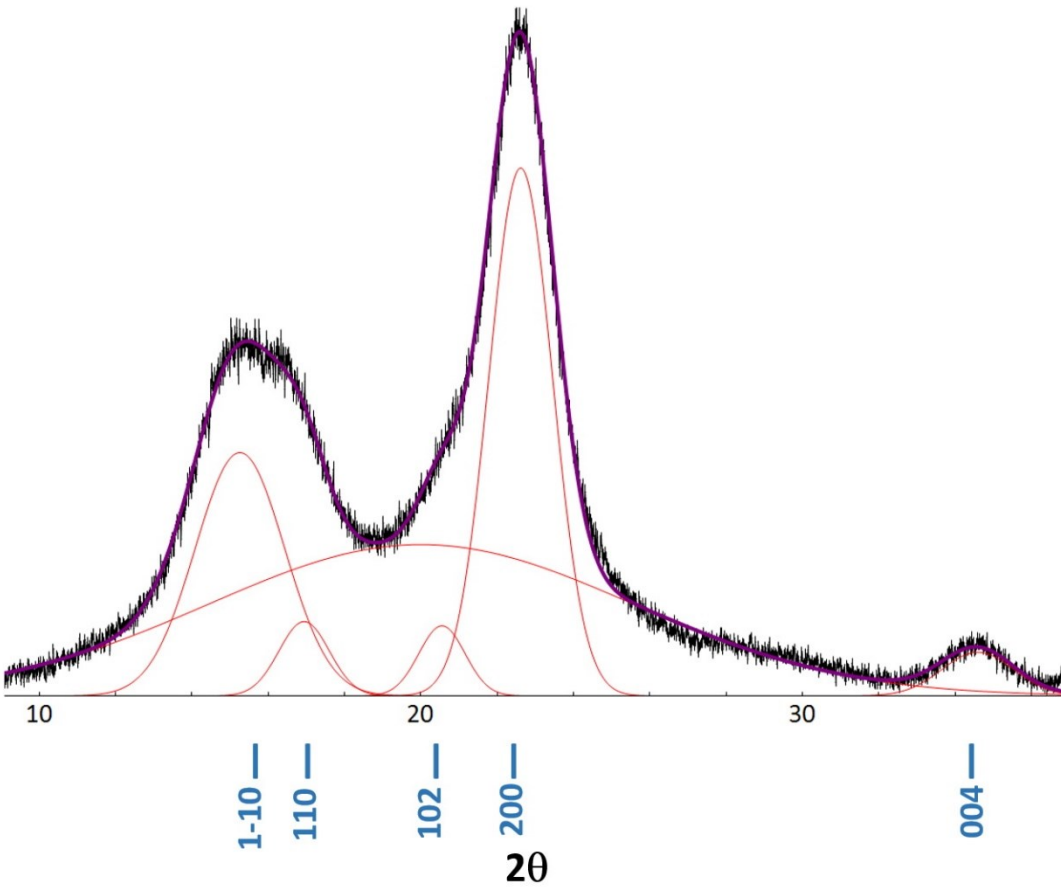

Fig. S30. XRD peaks deconvolution of Kraft cellulose treated with ChOAc:Im.

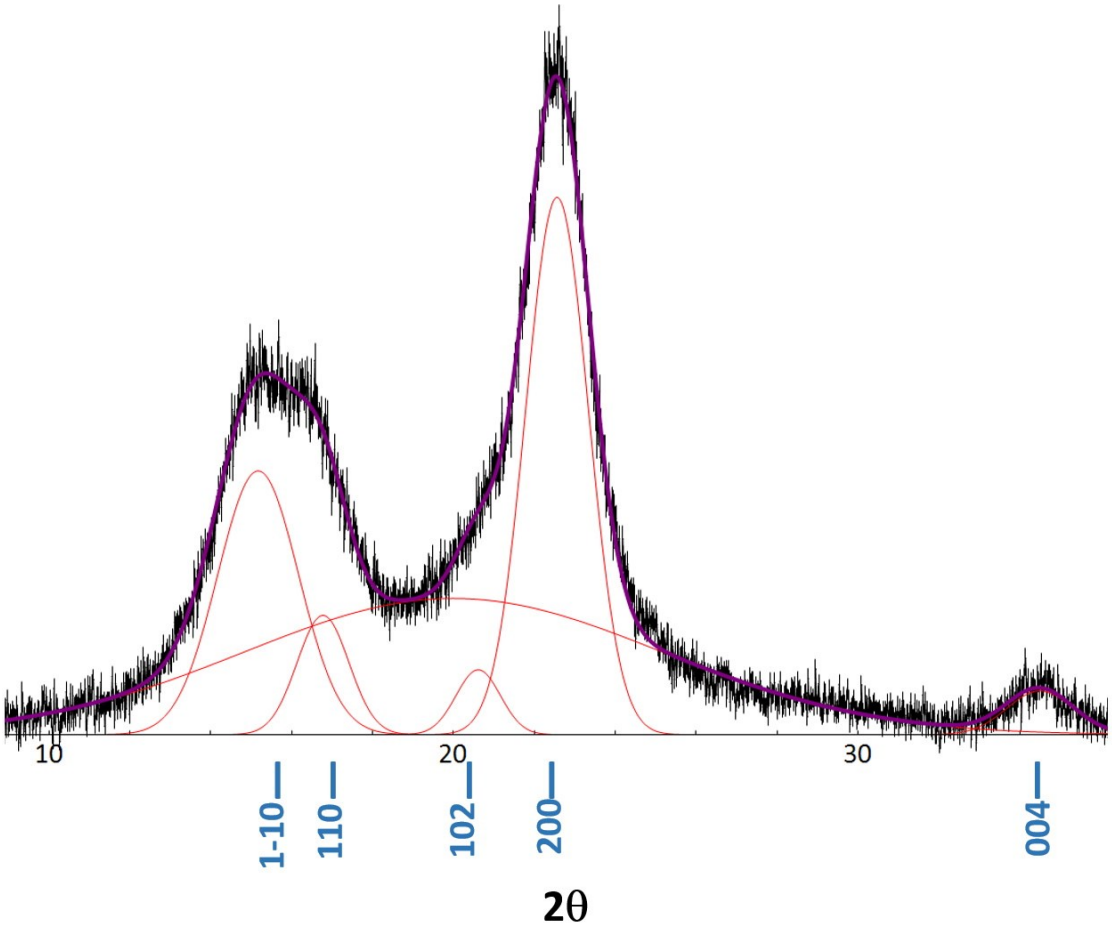

Fig. S31. XRD peaks deconvolution of Kraft cellulose treated with ChOAc:LevA.

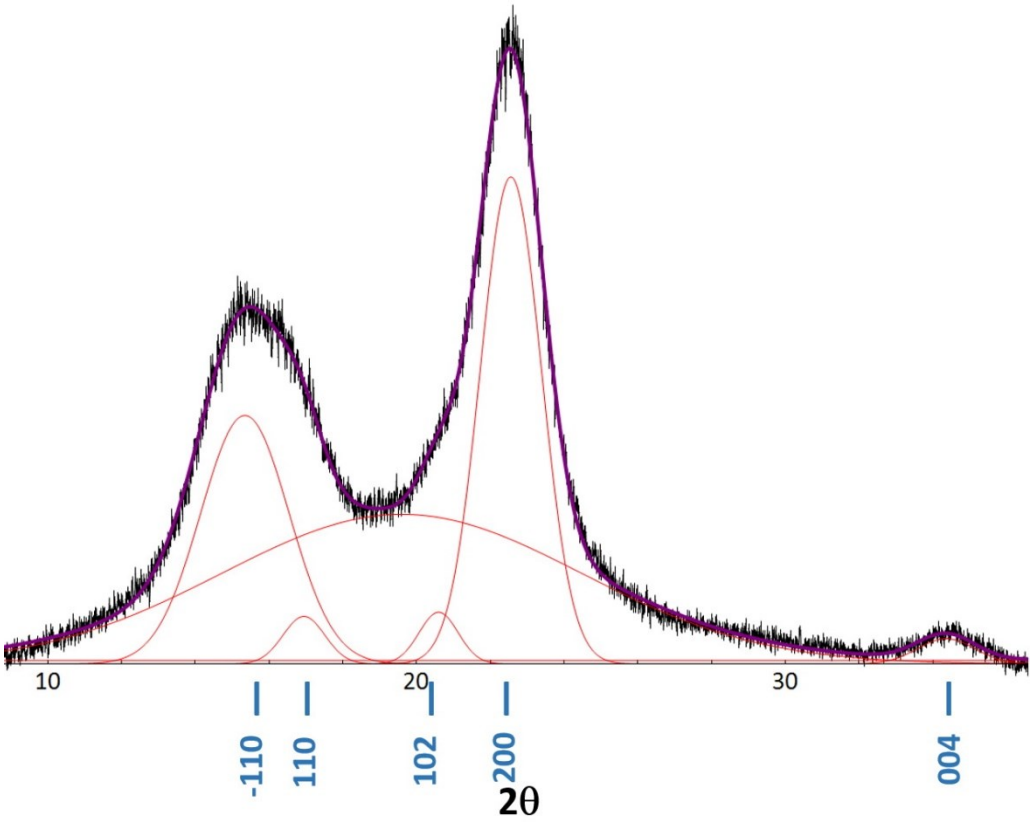

Fig. S32. PXRD peaks deconvolution of Kraft cellulose treated with ChOAc:LevA and 15 wt.% of water.

TGA

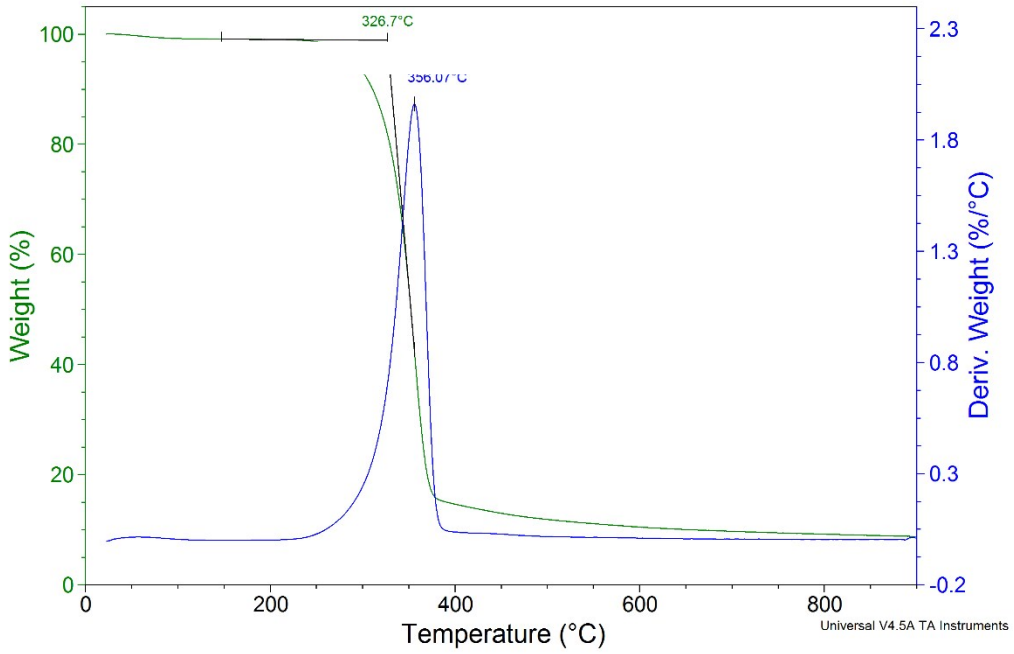

Fig. S33. TG curve of Kraft cellulose.

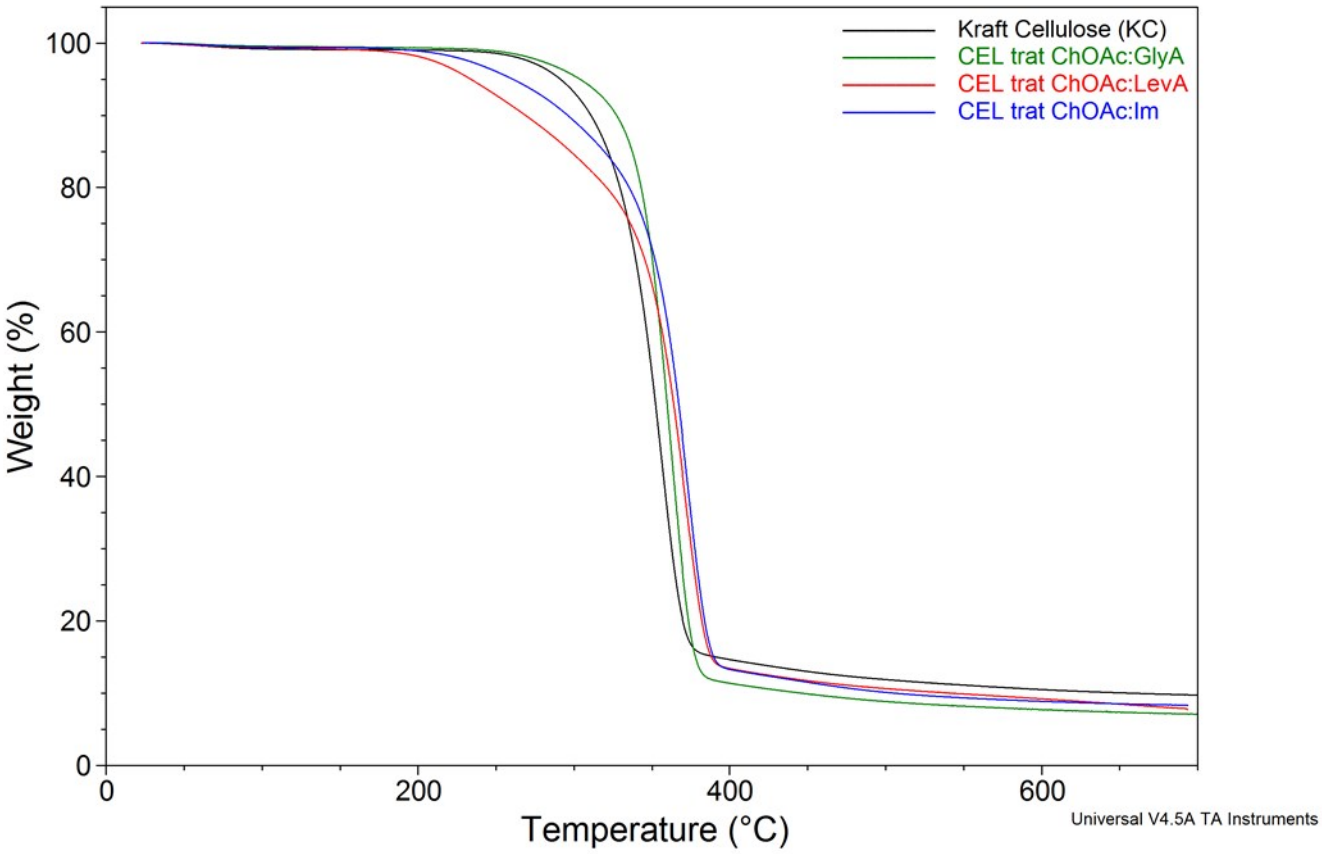

Fig. S34. TG curve of dissolved and regenerated Kraft cellulose (KC) compared to pristine KC.

IR

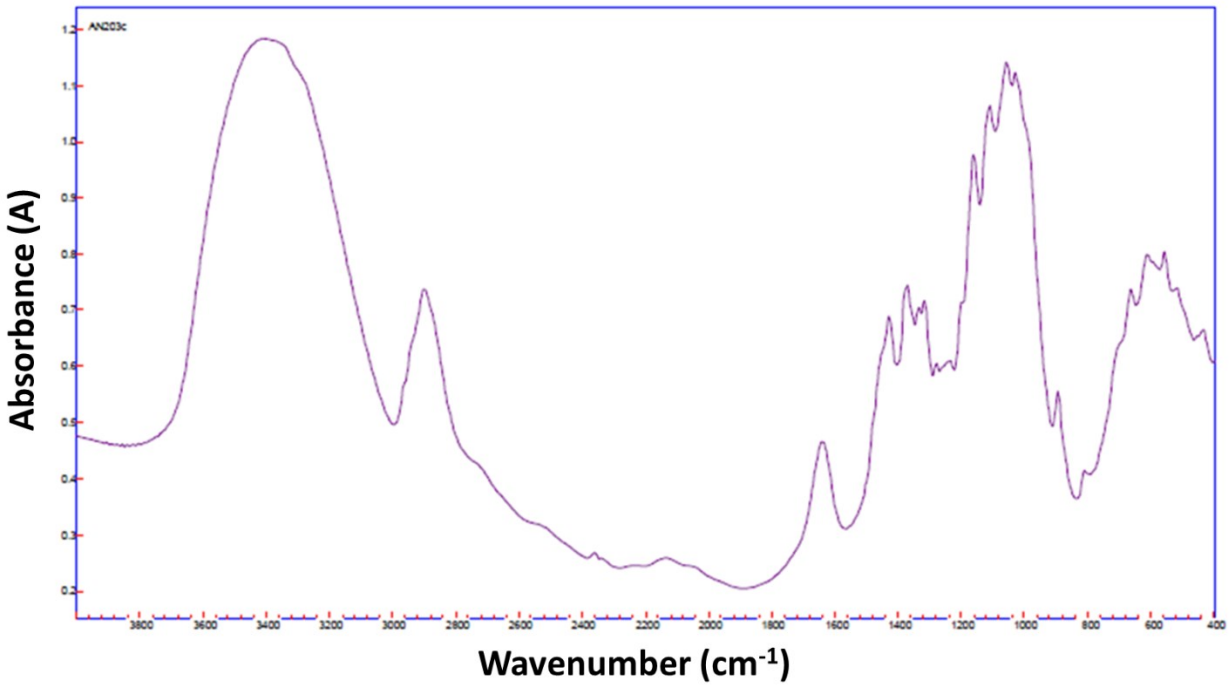

Fig. S35. FT-IR spectrum of Kraft cellulose.

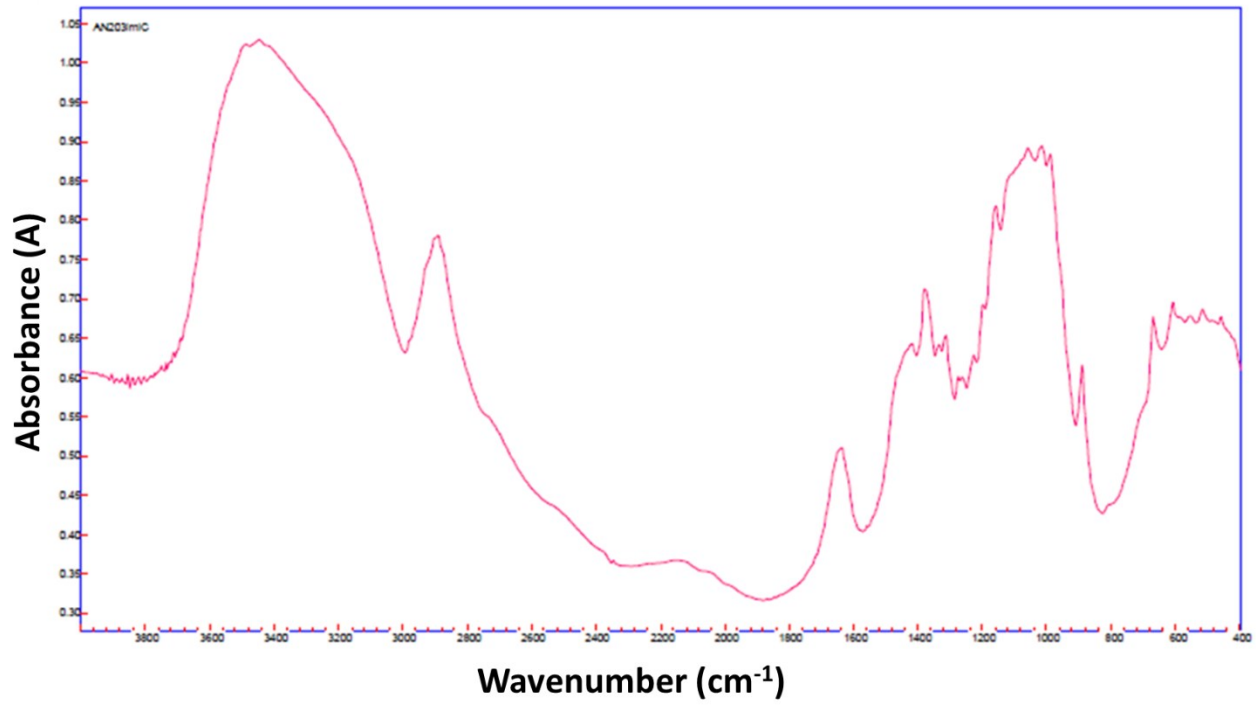

Fig. S36. FT-IR spectrum of Kraft cellulose treated by ChOAc:Im.

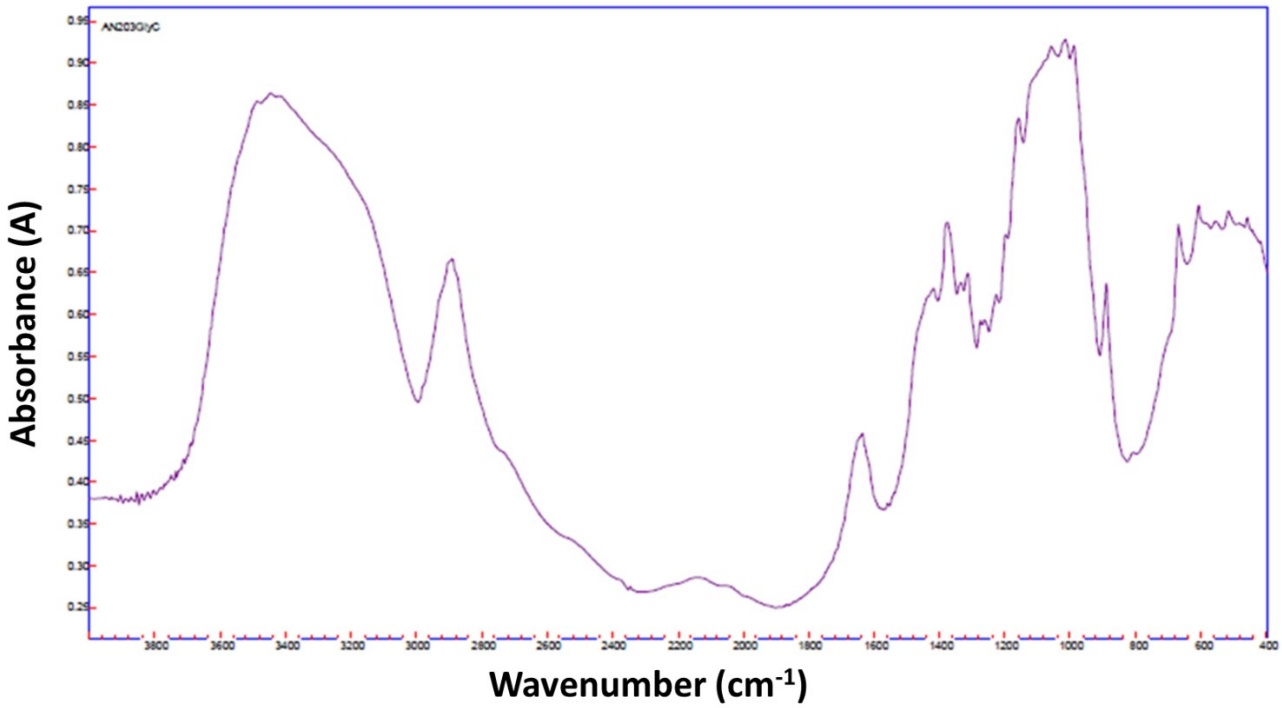

Fig. S37. FT-IR spectrum of Kraft cellulose treated by ChOAc:GlyA.

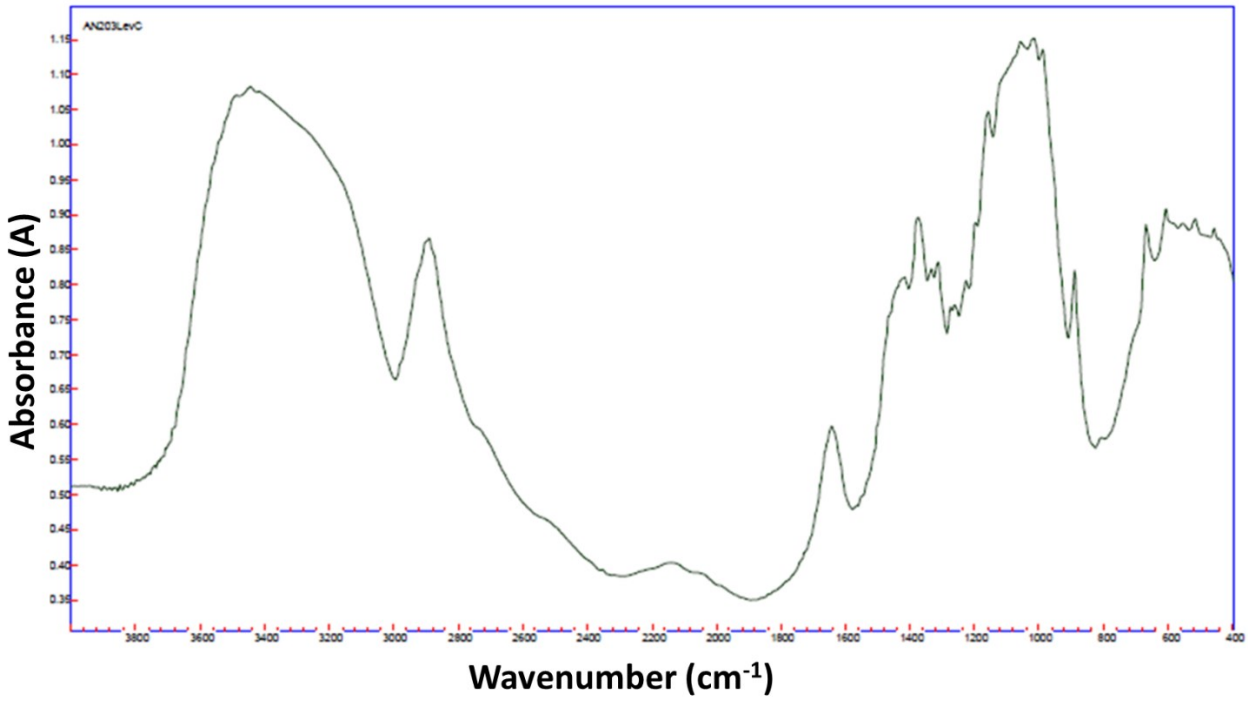

Fig. S38. FT-IR spectrum of Kraft cellulose treated by ChOAc:LevA.

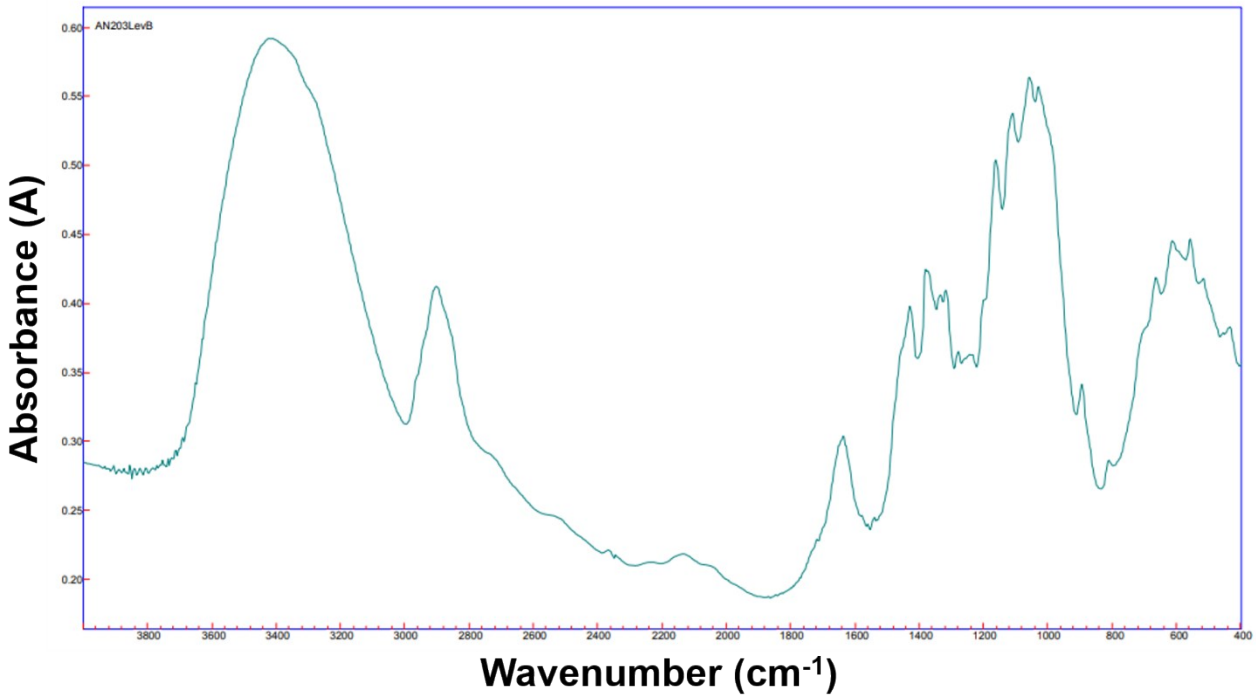

Fig. S39. FT-IR spectrum of Kraft cellulose treated by ChOAc:LevA+15wt%.

DES cost estimation and recycle

Table S5. Best quotation of raw materials for DES preparation.

	Cost* (euro/Kg)	MW
Choline Acetate	116.00	163.21
Imidazole	5.00	68.077
Choline Chloride 75% w/w	0.72	139.62
Acetic Acid 80% w/w	0.85	60.052
Levulinic acid	1.90	116.11
Glycolic Acid	8.00	76.05
NaOH	0.20	39.997
$ChOAc_{opt}$	1.495	163.21

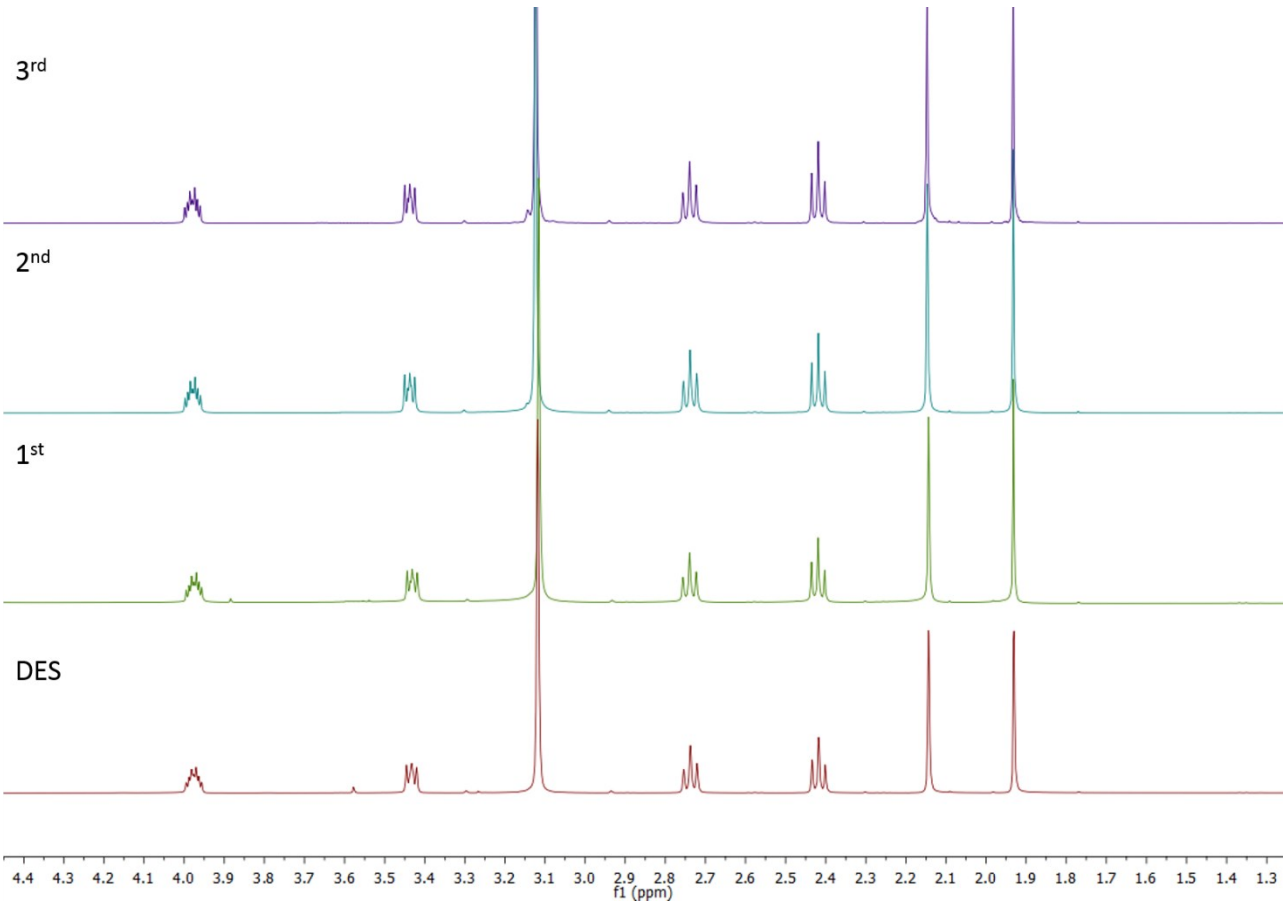

Fig. S40. ^{1}H NMR spectra of fresh and the recycled DES, ChOAc:LevA, at different DES cycles.

References

1 W. Chen, Z. Xue, J. Wang, J. Jiang, X. Zhao and T. Mu, *Wuli Huaxue Xuebao/ Acta Phys. - Chim. Sin.*, 2018, **34**, 904–911.

2 C. J. González-Rivera, E. Husanu, A. Mero, C. S. Ferrari, C. Duce, M. R. Tinè, F. D'andrea and L. G. Pomelli, *J. Mol. Liq.*, 2019, 10.1016/j.molliq.2019.112357.

3 M. R. Vignon and C. Gey, *Carbohydr. Res.*, 1998, **307**, 107–111.

4 H. Kim and J. Ralph, *RSC Adv.*, 2014, **4**, 7549–7560.

5 A. Teleman, M. Tenkanen, A. Jacobs and O. Dahlman, *Carbohydr. Res.*, 2002, **337**, 373–377.